Stratigraphic evolution and characteristics of lobes: a high-resolution study of Fan 3, Tanqua Karoo, South Africa.

by

J.M. Neethling

Thesis presented in partial fulfilment of the requirements for the degree of

Master of Science

at the University of Stellenbosch

Supervisors

Dr. H. de V. Wickens

Dr. D.M. Hodgson

March 2009

Geology

Stellenbosch University

Chapter 4

Application of Sequence Stratigraphy

Application of Sequence Stratigraphy

4.1 Introduction

Sequence stratigraphy is defined as “the study of rock relationships within a time-stratigraphic framework of repetitive, genetically related strata bounded by surfaces of erosion or non-deposition, or their correlative conformaties” (Posamentier *et al*, 1988; Posamentier and Vail, 1988; van Wagoner, 1995). The purpose of sequence stratigraphy is two fold: it is used to reconstruct the allogenic controls during deposition, and aids the prediction of lithofacies architecture in unexplored areas.

Whilst sequence stratigraphy was initially developed for shallow-marine environments, several authors (Gardner and Sonnenfeld, 1996; Sixsmith, 2000) have indicated that it can be just as useful in deep-water settings. However, the standard definitions used for sequence stratigraphy still refer to shallow-marine features, such as shelf and shoreline (Prélat, 2006). In order for these methods to be used for deep-water features, such as those found in Fans 1 through 4 in the Tanqua depocentre, the definitions need to be adjusted. Also, no Type 2 sequence boundary can be present in deep-water settings, as the definition relies on features found only in shelf environments, such as a basinward lithofacies shift. Type 1 sequence boundaries can be recognized in deep-water environments by the relative positions of more distal and more proximal features in relation to each other. These features can directly be related to an abrupt increase of sediment supply caused by relative fall in sea level and a loss of accommodation space, which results is a basinward shift in lithofacies (In other words: a more proximal feature will be directly above a more distal feature in the stratigraphy).

Boggs (2001) described depositional systems as being composed of successions of genetically related strata deposited under particular environmental conditions, the latter being associated with different parts of a cycle of relative rise and fall of sea level. These depositional sequences are known as system tracts. Prélat (2006) used the Exxon tripartite model as described by van Wagoner *et al.* (1988), which consists of highstand, lowstand and transgressive system tracts. Given the similarity between the Laingsburg and Tanqua depocentres, the same approach shall be used here.

Highstand System Tracts (HST) are formed during later stages of sea level rise. The early stage of HST in deep water is characterised by hemipelagic mud deposition. This is because of the increase in accommodation space, which ensures that almost none of the coarser sediments are transported beyond the shelf edge. Turbidites can however be deposited during HST in deep water if sediments can accumulate on the shelf edge.

Lowstand System Tracts (LST) are formed during relative sea level fall. They are characterised by a basinward shift in coarser sediment deposition. Gravity processes, such as sediment gravity flows, play an important role in moving sediment beyond the shelf edge.

Transgressive System Tracts (TST) are formed during that part of relative sea level rise when the rate of accommodation space increase exceeds the rate of sediment supply into the basin. A TST is characterised by basin filling, and is contained within basinal mudstone in deep water.

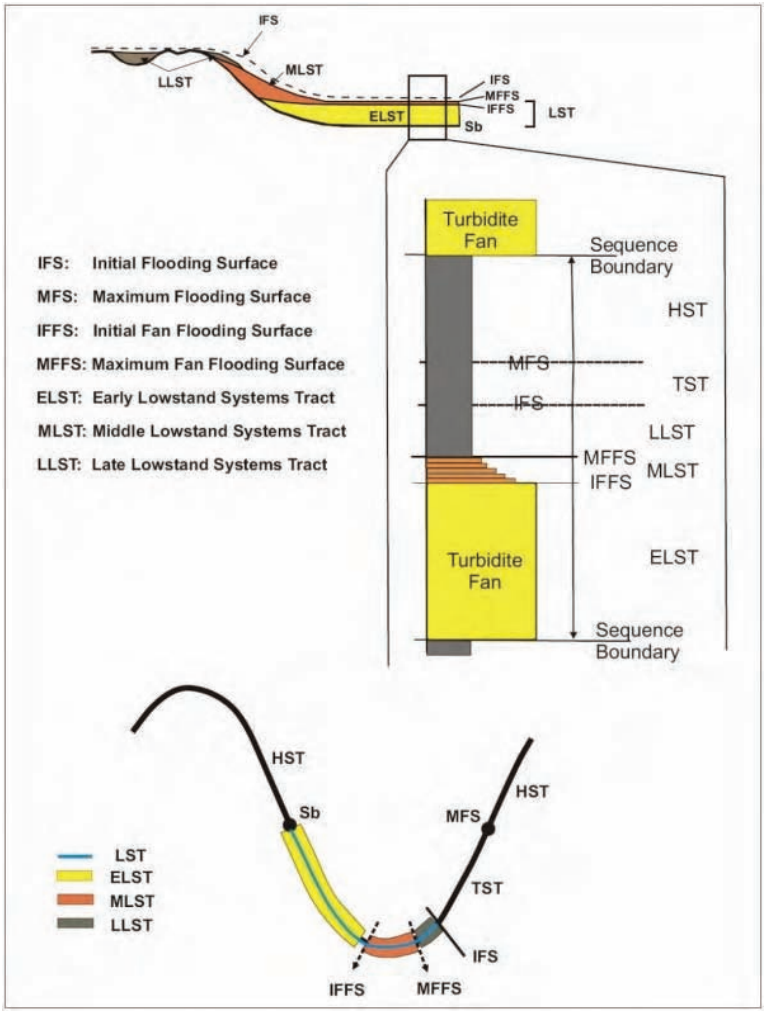

Figure 4.1 A simple diagram from Sixsmith (2000) showing the surfaces and zones used to describe a turbidite.

Sequence boundaries are fairly easy to recognise in deep water settings, as they are on average regionally extensive and are characterised by abrupt changeover from hemipelagic claystone and siltstone to sandy material. Fan 3's base sequence boundary vary between relatively abrupt changeovers from clay to sand, and more gradual changeovers where claystone grades into gradually thickening siltstone units, and eventually sandstone. In general however, it is highly likely that the boundaries are not sharp, showing the gradual changeover from mud to silt to sand. In seismic profiles, the sequence boundaries would appear sharp, but in reality they probably have a vertical extent of up to several meters, which is below the resolution of general seismics.

Marine flooding surfaces in deep water environments can be distinguished as a mudstone succession above a sandstone succession, indicative of starvation, as the rise in sea-level causes a shift in sedimentation out of the deep basin. The Initial Fan Flooding Surface (IFFS) can be seen as the top of the last sandstone succession in Fan 3, namely Lobe 6. As the top of the fan is very rarely well exposed in the study area, it is difficult to see the Maximum Fan Flooding Surface (MFFS) in outcrop, and near impossible to locate the Initial Flooding Surface (IFS) and Maximum Flooding Surface (MFS), located in the muds above the fan. Where it is exposed, the MFFS is an upward fining succession of siltstones, grading into claystone. The Bouma succession is rarely present in its entirety. The different flooding surfaces mentioned above are based on the definitions as described by Sixsmith (2000). The basic concepts are shown in the diagram of Figure 4.1.

4.2 Application

The application of the sequence stratigraphy principles on Fan 3 is displayed in Figure 4.2. Based on the descriptions of Sixsmith (2000, Fig. 4.1), the sequence boundaries have been placed at the stratigraphic base of both Fan 3 and Fan 4 (top of image). The description by Sixsmith assumes only a single Bouma sequence. However, Fan 3 consists of several incomplete Bouma sequences, every lobe and lobe-element showing a Ta to Tb/Tc pattern, with Td present only between them, and Te only above the lobe complex. Given the eroded nature of the Te succession between Fan 3 and Fan 4, the relative positions of the MFFS, IFS and MFS are only estimates, their true positions impossible to determine from these outcrops.

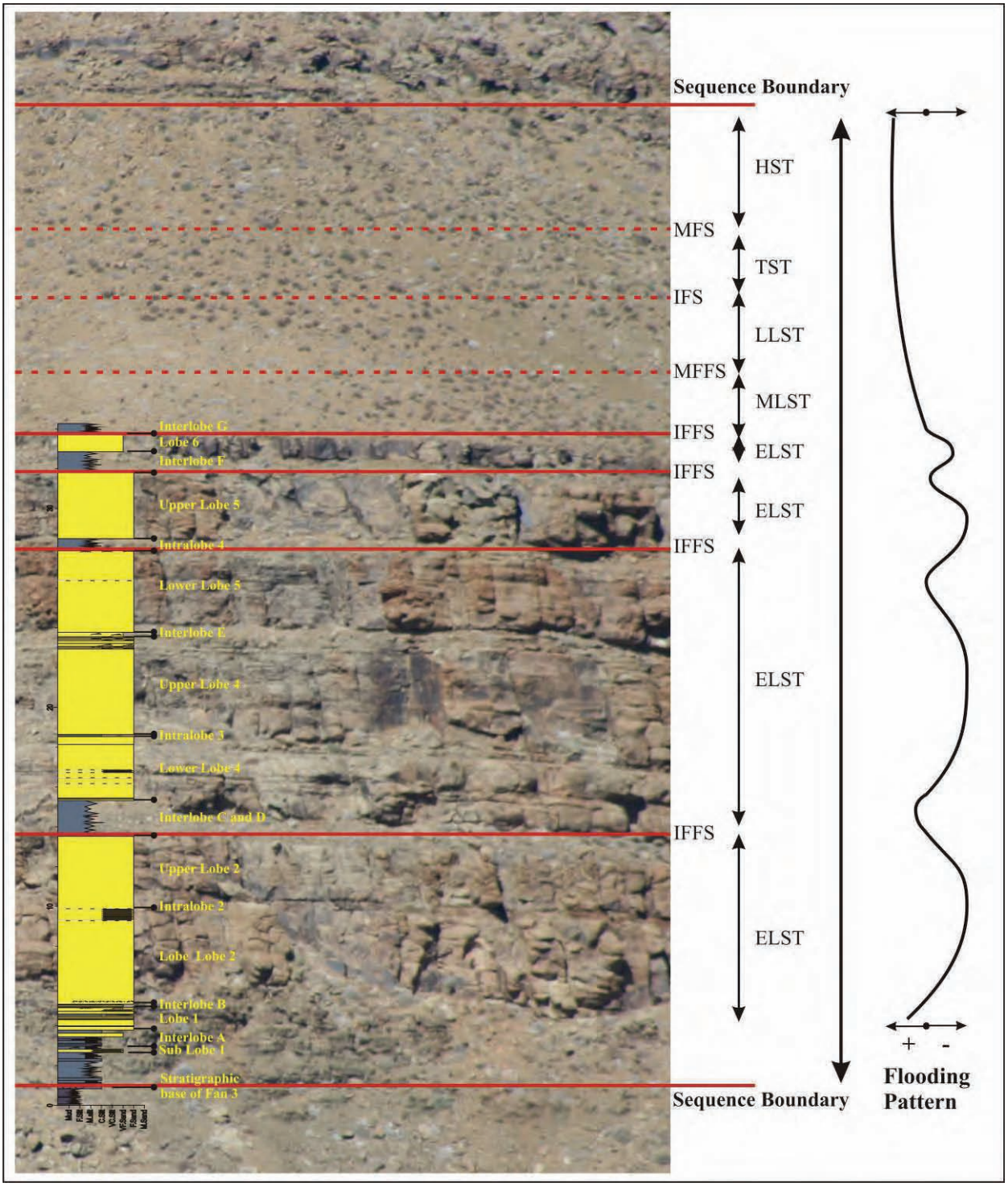

Figure 4.2 Application of sequence stratigraphy on the outcrops of Fan 3 of the southern Gemsbok River valley.

Assuming some allogenic control over lobe deposition, a general pattern of sea-level fluctuation can be inferred. The entire lobe complex was deposited during LST (relatively shallower sea-level). On a more micro-scale, internal variation within the lobe complex shows a

pattern of variable flooding. Lobes and lobe-elements were each deposited during an early LST (ELST) followed by fine-grained deposition after an initial fan flooding surface (IFFS).

The lengths of the flooding stages correspond to the progradation-aggradation-retrogradation pattern as described by Hodgson *et al*. (2006) for Fan 3. Fig. 4.3 is a dip section schematic of the outcrops to the south of the Gemsbok River valley to the northern pinch-out of Fan 3. The figure was modified from Prélat *et al*. (in review) in order to show both Upper and Lower Lobe 4. Lobe 5 was left unchanged, as Upper Lobe 5 has a similar pattern to Lobe 6. The red box represents the observed outcrops of this study (the area south of the Gemsbok River valley). The figure is not drawn to scale. The Sub Lobes and Lobes 1 and 2 represent the progradational phase, or initial basin-ward shift of Fan 3. Lobes 4 through Lower Lobe 5 are aggradational, gradually building the bulk of the fan. This part constrains the largest part of the fan, in terms of thickness and spatial and volumetric extent. Upper Lobe 5 and Lobe 6 are more retrogradational, at least this is their appearance in the study area. Their thickness never matches that of the underlying lobes, which are much thicker down-dip. Also, Lobe 6 pinches out over almost 6 kilometres along the Gemsbok River valley, but has only a single identified axial zone and remains mostly structured away from this zone.

The above pattern is also reflected on the micro-scale. The length of the gradation stages determined the duration of the ELSTs, and as a result the volume of the lobes that were deposited during that stage. To illustrate this graphically, a line diagram is presented on the right in Fig. 4.2. A curve to the right means a relative lowering of sea-level, where as a curve to the left is a relative increase in sea-level. It should be noted that the longest ELST is again an

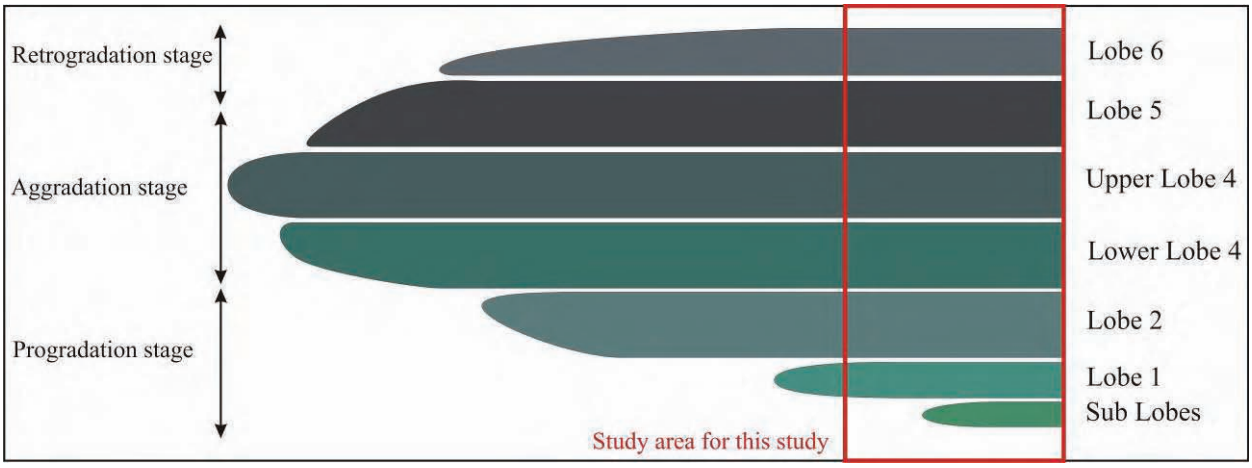

Figure 4.3 Schematic of a dip section through mid to distal Fan 3 to illustrate the different stages of deposition. Modified from Prélat *et al*. (in review).

average, as Lower Lobe 5 is amalgamated to Lobe 4 in this location (Profile J0820250LK). In other words, an IFFS should be present between them. However, Lower Lobe 5 is still aggradational. Therefore the relative rise in sea-level in the interval between the deposition of Lobe 4 and Lower Lobe 5 would have been minor.

Chapter 5

Data Manipulation

Data Manipulation

5.1 Introduction

Large amounts of data were gathered during the fieldwork sessions. Before the data can be analysed and manipulated, however, it has to be organised and prepared for each requirement.

The data were gathered in the field using standard vertical profiles (also referred to simply as logs) measured on a centimetre scale. 72 of these profiles, varying in thickness from 15 to 40 metres, were collected. These profiles distinguish between grain-size, lithofacies and unit thickness, and also indicate observed sedimentary features and paleocurrent measurements. Combined with high-resolution digital photometry, the data provide detailed information of the study area. In order to use these data in computer programs, the data had to be digitized using programs such as DSL and Microsoft® Excel 2003.

5.2 Digitisation of data

CorelDraw X3

The first part of the digitization process was to convert the logs into CorelDraw X3. This is not merely to have a visual representation of the data, but also to more easily trace out the individual bed-sets, lobe-elements and lobes, as observed in the field and on the digital photos. This was used as the basis for distinguishing between the lobes and lobe-elements of Fan 3 (Chapter 3), and by extension the basis for sorting the data for use in Petrel. It is also a useful method for displaying the palaeocurrent rose-diagrams used to analyse the palaeoflow patterns. Several correlation panels were created using this method. These incorporate all 72 profiles and are displayed in Chapter 3.

Microsoft Excel 2003

Spreadsheets were used to represent the data and to calculate several features accurately (and quickly). Given the inaccuracy of handheld GPS receivers (errors vary from 3 to several tens of

metres), only the top GPS coordinates were used to reference the positions of the profiles, as they are generally more accurate and display smaller errors (better overhead coverage). For this reason, the bottom coordinates, as well as the tops and bottoms of every bed in relation to the top GPS coordinates, were calculated in Excel for later use. GPS measurements were taken using UTM standards.

The data gathered in the field proved more difficult to use in Petrel than expected. None of the lobes had the same regional extent (E-W and N-S extent). Figure 5.1 shows an example of what the final spreadsheets looked like. It shows the tops and bases of all individual lobes and lobe-elements defined for use in Petrel. These numbers were calculated by subtracting measured thicknesses from the topmost GPS coordinate.

Profile Name	X Coordinate	Y Coordinate	Top	Top L6	Base L6	Top UL5	Base UL5	Top LL5	Base LL5	Top UL4	Base UL4	Top LL4	Base LL4
J7030245RD	412255	6385599	**568**	568.00	558.85	558.31	558.31	557.77	555.91	554.56	552.56	552.36	552.36
J6830263RD	411967	6385745	**561**	563.30	561.40	561.20	561.20	561.00	559.53	559.53	556.96	556.76	556.76
J6450245RD	411817	6385234	**586**	586.00	582.51	581.46	581.46	580.41	578.56	578.24	575.69	575.49	575.49
J6180245ZM	411553	6385156	**593**	593.00	586.80	586.00	586.00	585.19	583.59	583.39	581.39	581.19	581.19
J5940245ZM	411283	6385083	**582**	581.30	574.13	573.16	573.16	572.18	570.23	569.69	567.69	567.49	567.49
J5030246ZM	410522	6384661	**567**	567.00	562.28	561.73	561.73	561.18	557.89	557.39	554.83	554.63	554.63
J4930248ZM	410499	6384466	**576**	576.00	571.03	570.50	570.50	569.96	565.84	565.12	562.34	562.14	562.14
J4860243ZM	410236	6384795	**556**	558.30	556.40	556.20	556.20	556.00	551.14	550.46	546.74	546.54	546.54
J4800242ZM	410181	6384778	**560**	560.00	559.20	558.90	558.90	558.59	553.91	553.47	547.79	547.59	547.59
J4710243ZM	410103	6384732	**560**	562.30	560.40	560.20	560.20	560.00	556.07	555.53	551.31	551.11	551.11
J3730245ZM	409310	6384105	**567**	567.00	564.05	563.53	563.53	563.00	558.64	558.04	553.32	553.12	553.12
J3570245ZM	409185	6384023	**572**	572.00	568.79	568.41	568.41	568.02	565.24	564.79	559.67	559.14	558.32
J3430245ZM	409052	6383961	**568**	568.00	564.74	564.05	564.05	563.35	559.63	558.82	552.30	552.11	550.21
J3270245ZM	408888	6383941	**571**	571.00	570.36	569.95	569.95	569.54	564.74	564.11	557.76	556.89	556.32
J3150245ZM	408815	6383872	**569**	571.30	569.40	569.20	569.20	569.00	565.26	564.66	556.76	556.76	553.56
J2920246ZM	408596	6383745	**563**	567.40	565.50	565.30	565.30	565.10	563.20	563.00	557.59	556.67	554.32
J2760256ZM	408578	6383217	**550**	550.00	548.34	548.30	548.30	548.26	544.96	544.96	539.66	539.66	538.33
J2750246ZM	408435	6383682	**565**	569.40	567.50	567.30	567.30	567.10	565.20	565.00	563.59	563.00	559.76
J2690255ZM	408512	6383242	**555**	557.30	555.40	555.20	555.20	555.00	550.80	550.28	545.38	545.38	543.50
J2660254ZM	408482	6383272	**552**	556.40	554.50	554.30	554.30	554.10	552.20	552.00	546.68	546.68	545.66
J2340249ZM	408094	6383398	**576**	580.40	578.50	578.30	578.30	578.10	576.20	576.00	572.41	570.74	567.68
J2130246ZM	407872	6383410	**589**	591.10	589.20	589.00	588.44	588.11	585.24	584.76	581.77	581.67	577.67
J2030246ZM	407788	6383363	**593**	593.00	592.22	591.18	590.35	589.98	587.65	587.03	582.87	582.49	579.07
J1930246ZM	407670	6383315	**601**	601.00	599.41	598.21	597.55	597.08	594.00	593.16	589.87	589.64	585.34
J1800247ZM	407605	6383233	**607**	607.00	605.30	603.68	602.75	602.00	599.98	599.25	596.21	595.84	592.04
J1700248ZM	407517	6383184	**602**	604.10	602.20	602.00	601.72	601.35	597.46	597.09	594.10	593.80	588.25
J1600248ZM	407427	6383149	**609**	611.60	609.70	609.50	609.02	609.00	604.44	603.80	599.66	599.08	595.22
J1500248ZM	407332	6383110	**617**	619.10	617.20	617.00	616.31	616.11	613.01	612.46	606.62	606.42	604.52
J1400247ZM	407237	6383062	**628**	628.00	625.20	623.74	622.74	622.20	619.10	618.57	613.95	613.78	610.51
J1300248ZM	407143	6383021	**633**	632.80	630.54	629.70	628.80	628.50	624.41	624.41	620.62	620.62	618.82
J1200249ZM	407058	6382967	**636**	636.00	634.55	633.53	631.63	631.23	629.15	629.15	623.55	623.55	621.85
J1100249ZM	406984	6382993	**637**	637.00	636.20	635.18	632.72	632.52	630.98	630.98	629.09	629.09	623.76
J1030252ZM	406903	6382875	**635**	635.00	634.10	632.97	630.51	630.16	627.46	627.46	622.16	622.16	619.33
J0920253LK	406808	6382816	**625**	625.00	624.20	623.04	620.14	619.95	615.30	615.20	610.55	610.35	608.45
J0820250LK	406709	6382801	**622**	621.52	620.58	619.52	616.22	615.61	612.11	611.89	606.97	606.87	603.72
J0620258LK	406552	6382653	**626**	626.00	626.00	625.80	623.76	622.94	618.69	618.65	617.15	616.95	612.86
J0450266LK	406396	6382558	**616**	618.30	618.30	618.10	616.20	616.00	611.97	611.97	609.33	609.13	605.96
J0350269LK	406277	6382534	**615**	619.40	619.40	619.20	617.30	617.10	615.20	615.00	612.20	612.20	608.80
J0100292LK	406025	6382520	**623**	625.30	625.30	625.10	623.20	623.00	622.43	622.33	619.68	619.68	616.80
J0000000LK	405933	6382519	**625**	625.20	625.20	625.00	624.45	624.33	622.31	622.31	620.41	620.41	616.31
J0500312LK	406350	6382216	**574**	578.40	578.40	578.20	576.30	576.10	574.20	574.00	570.54	570.54	570.19
J0560002LK	405949	6381967	**604**	606.30	606.30	606.10	604.20	604.00	600.82	600.82	598.66	598.66	598.14
J0500345LK	406102	6382069	**598**	600.30	600.30	600.10	598.20	598.00	591.96	591.96	589.96	589.96	588.16
J0950345LK	406185	6381585	**585**	587.10	585.20	585.00	583.80	583.63	572.78	572.58	571.93	571.93	571.28
J0950357LK	406005	6381558	**576**	578.10	576.20	576.00	574.08	573.92	566.88	566.68	566.16	566.16	565.63
J1270348LK	406227	6381286	**578**	582.20	580.30	580.10	578.20	578.00	576.51	576.51	573.49	573.49	571.49
J1330352LK	406145	6381193	**578**	582.20	580.30	580.10	578.20	578.00	572.01	571.81	570.83	570.83	569.85
J1490345LK	406359	6381089	**583**	587.20	585.30	585.10	583.20	583.00	581.74	581.61	579.13	579.13	577.42

Figure 5.1 Part of one of the spreadsheets used to calculate top and base values for use in Petrel. The yellow cells represent areas where no data were present in the initial construction of the spreadsheet. The values were calculated during the later stages of modelling in order to facilitate the process in Petrel.

The yellow cells in Figure 5.1 represent areas where no data were present in the field, i.e. either through lack of outcrop, erosion or pinch-out, or where lobe-sets were too amalgamated to separate (between white cells). The values in these cells were calculated in order to give all lobes the same regional extent. This makes using them in Petrel a lot easier.

In general, one basic rule was followed: the thickness of the siltstones-breaks separating lobes were set to 20 cm in areas where no outcrop data were present. To keep things simple, it was assumed that the sandstones were amalgamated, which is probably not far from reality.

In some cases the sand-prone lobes pinched out. For these instances the 20 cm siltstone breaks

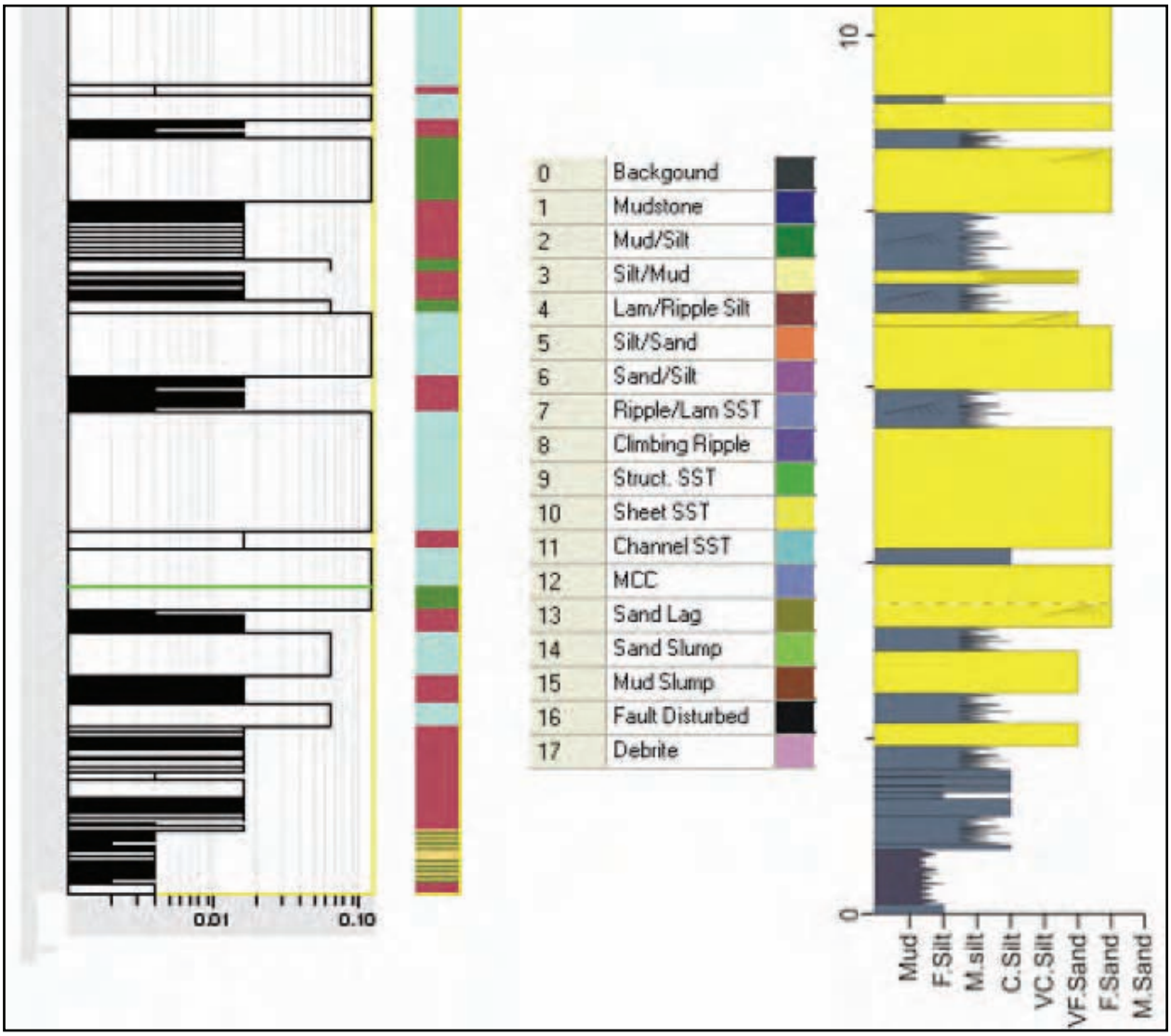

Figure 5.2 An example of how DSL (left) and CorelDraw (right) displays the same vertical profile, in this case J4930008LK. DSL's digital usage of data makes it very useful for exporting into other programs, whereas CorelDraw provides a better visual display of the data.

were again used, but the top and base values for the lobes were made equal. This ensures that the lobes are still “present”, but forms a flat surface. The result of all this was that all the profiles could be included in Petrel, as they now had the same regional extent.

It should be noted that these steps were only taken during the later stages of the Petrel modelling.

DSL

DSL is a versatile in-house program developed by D. Hodgetts in 2001 (now at University of Manchester) and used by the University of Liverpool. It is capable of recording and displaying a great variety of data associated with vertical profiles. It is also capable of exporting this data in several formats which can be used by Petrel. DSL was used to digitize the field data in such a way as to record the beds and their individual lithofacies, as well as the top and bottom GPS coordinates for each profile. In order to avoid confusion, the profiles will from here on be referred to as “wells” or “well logs”, as this is how Petrel refers to them. For the same reasons mentioned above, and in order not to import inclined wells into Petrel, the bottom GPS coordinates were set the same as the top coordinates, and the bottom depth was set as the calculated depth from the Excel spreadsheets. The data were exported for Petrel as RMS well logs. RMS is a different program which can also be used for modelling. The format is supported by both Petrel and DSL, which makes it a very useful format.

Figure 5.2 is an example of the different ways DSL and CorelDraw display the wells. While CorelDraw displays the same data, it cannot be exported in any useful format, whereas DSL has all the data in digital format already. Also, in Fig. 5.2 it should be noted that DSL uses 17 lithofacies, whereas only 5 lithofacies and lithofacies associations were discussed in Chapter 3.

The reason for this is simplicity: where DSL refers to two or more variations of siltstone-to-claystone and sandstone-to-siltstone ratios, these were grouped as siltstones and structured sandstones in the lithofacies descriptions (and later in Petrel). Also, not all of the DSL lithofacies were used. Only those applicable to or comparable with the lithofacies as described in Chapter 3 were used. A more detailed description of this process is provided in Chapter 7.

All 17 of these lithofacies were imported “as is” into Petrel, because the file type used to import the wells uses a number-based text system. In other words, every feature is assigned a

number and placed in a certain location in a tab-delimited text table. The lithofacies are numbered 0 through 16. In order for Petrel to import them correctly, the defined lithofacies in Petrel have to match the lithofacies in DSL. For example, before all the lithofacies were imported, structureless sandstone imported incorrectly as carbonates. The issue is solved by creating a custom lithofacies list that corresponds to the DSL lithofacies list (See Chapter 7 for a detailed description of this process).

As a comparison between the different ways in which Petrel and CorelDraw display a correlation panel, Appendix D shows a set of five of these panels as generated by Petrel. Figures D.1 and D.2 represent the first 11 wells at the start of outcrop (west to east, looking north), and Figures D.3, D.4, and D.5 correspond to Panels 1 – 2, 3 and 12 respectively. These panels are not accurate representations in terms of vertical scale, as each well was automatically adjusted by Petrel to show the same height, and not the true height. The first two panels use the original data, whereas the last three use the adjusted data (visible near the base of the panels as tight groupings of lines).

Chapter 6

Deposition of Fan 3

Deposition of Fan 3

6.1 Introduction

This chapter will attempt to explain some of the depositional features described in previous chapters, particularly Chapter 3. The 2D outcrop maps will be used in conjunction with the isopach maps generated in Petrel.

A "fan" is not the immediate result of a turbidity deposit, but rather the combination of many smaller events. A study by Machado *et al*. (2004) outlined three distinct deposits (based on age

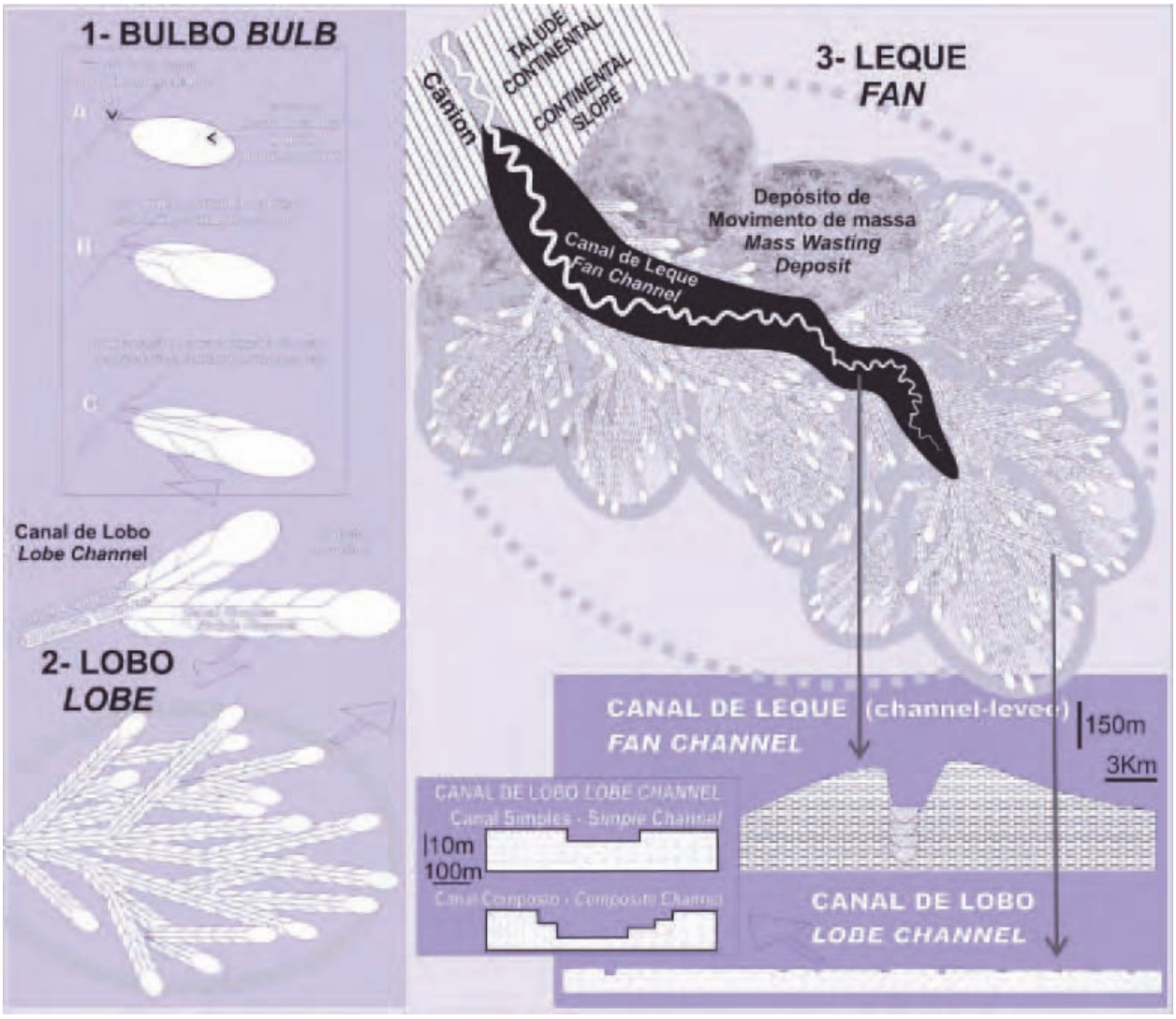

Figure 6.1 Three depositional models for turbidity currents as suggested by Machado et al. (2004). These models are based on age and complexity. Initially, a turbidity current forms a bulb. Given time and a constant sediment supply, several bulbs can build a lobe.

and complexity) based on studies of the modern Mississippi, Amazon and Indus deltas, as well as the Paraíba do Sul/ Carapebus (Fig. 6.1). These deposits can build upon themselves in order to form the larger deposits. In other words, several relatively small "bulb" deposits (singular turbidity flow deposits, equivalent to beds and even lobe-elements) can form a lobe channel. If enough of these lobe channels are present, a "lobe" can form. A fan is then the final product of several lobes stacked together. As an ancient analogy the Tanqua Fan Complex is a prime example.

6.2 Finger-shaped deposits of Fan 3

The pattern suggested by Machado *et al*. (2004) gives lobes a more "finger-like" appearance near the distal parts and margins, as opposed to a "classic" lobe shape. These features are shown in Figure 6.1. Several such features have been observed by the Liverpool teams to the north of the Gemsbok River, closer to the pinch-out of Fan 3 (Prélat *et al*., in review). These features are present in Lobes 4, 5 and 6, the last lobes to pinch out. In outcrop, they appear as major thickenings of a lobe after a steady thinning. They can appear within less than a hundred metres, and disappear just as fast, thickening a lobe by several metres within a very short distance (up to 8 metres within less than a hundred metres in the study area).

Figure 6.2 Example of the bedded nature of the finger-shaped axial zones. The correlated section at the top can be traced for hundreds of meters along strike, whereas the "extra" section at the base is very localised, with less than a hundred metres lateral extent. Note the large amount of mud-clast conglomerates at the top of the thickest sandstone. Here it resembles a debrite, with significant amounts of organic material.

Generally, these features are well structured (Fig. 6.2), with beds and lobe-elements clearly defined and separated by siltstone or claystone (mostly claystone, whereas the rest of the lobe is separated almost exclusively by siltstone). They can also appear as structureless sandstone, with large concentrations of dewatering features. What they all have in common are the mud-clast conglomerates, located at the top and above the thicker sandstones, and the lack of major scouring at the base. In the study area this thickening would erode less than 2 metres compared to more than 8 meters of thickening. It should be noted that the outcrop in Fig. 6.2 did show more than 2 metres of erosion, however, this was into the underlying muds, and not into sandstones. Nowhere in the study area do these features (the axial zones in the central section) erode into older sandstone units.

Also, some display features that resemble a squeeze effect, where mud or sand is forced into plastic (soft-sediment) deformation by a relatively sudden increase in overburden. To the north, these features were observed within the lobe. In the study area, one such feature was identified in the claystones 2 metres below the thickest sections of sandstone. Figure 6.3 shows such a feature, located in the claystones below the lobe.

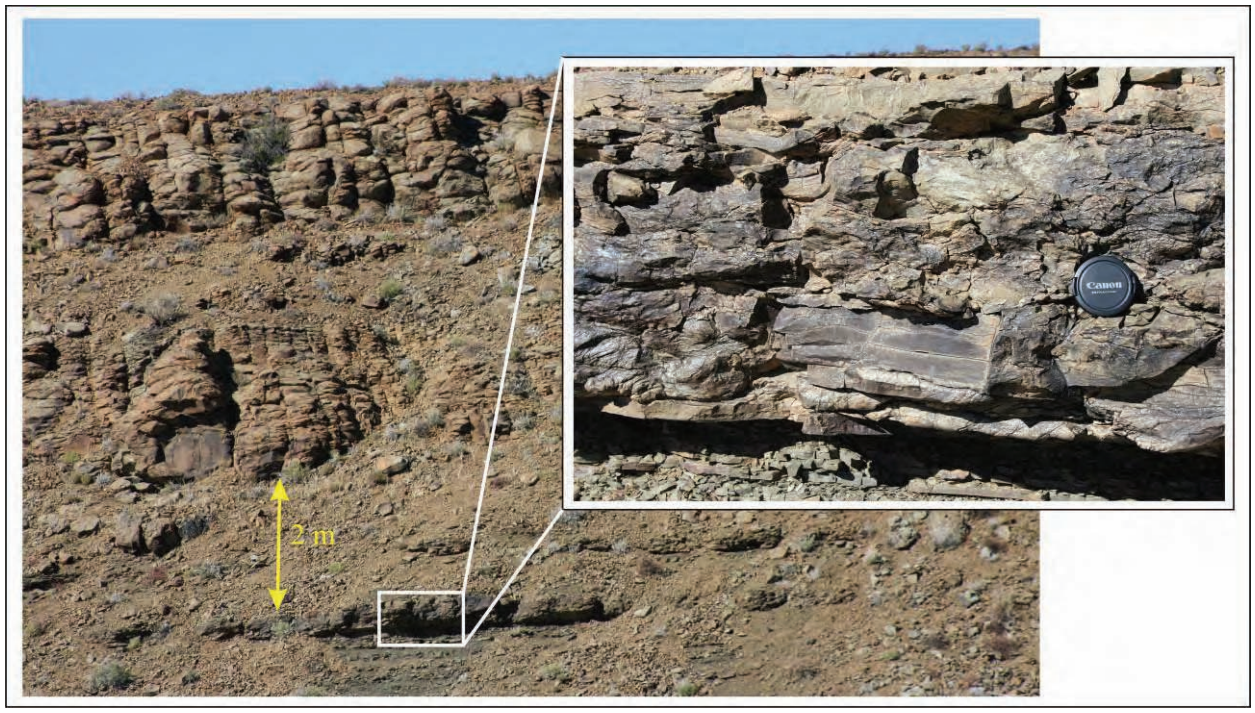

Figure 6.3 Example of the plastic (soft-sediment) deformation observed in the units below a finger-shaped axial zone. This example is a siltstone located in the claystones about 2 meters below a significantly thickened lobe (Upper Lobe 4).

6.3 Isopach maps

Isopach maps (also referred to as thickness maps) can be created in several ways in Petrel, though only two methods were used here. Petrel can create thickness maps automatically, or it can be instructed to subtract the Z-values of one surface from another. The end results are exactly the same: images showing the spatial variation in thickness between two surfaces. These results are best viewed in 2D. For a full description on how the data were manipulated and prepared for the creation of isopach maps, please refer to Chapter 5. Surfaces and their creation are described in Chapter 7, as they formed an integral part in the iterative process of modelling. All the isopach maps generated in Petrel are presented in Appendix C. These also indicate the known margins of lobes, as well as known axial zones, as determined in Chapter 3.

Two sets of isopach maps were created. Initially, the five different polygons were used, but this method did not allow the creation of isopach maps for the siltstone breaks. Using the newly calculated values for the “missing” tops and bases (some of which can be seen in Fig 6.1), the siltstone breaks can also be displayed. Their tops are the bases of the overlying lobes, and their bases the tops of the underlying lobes.

The initial isopach maps were each created with a different vertical scale (automatically adjusted) in order to better display the local variations for each unit (Fig. 6.4 A). The later isopach maps all used the same polygon; therefore their numbers increased from 10 to 19 in order to include the siltstones (Fig 6.4 B). Most of them used a fixed vertical scale to better compare them. This scale for sandstone prone lobes and lobe-elements had to be reduced for lower units, as their drastic decrease in thickness meant they were no longer comparable to the upper units.

As an example of how the original data (in CorelDraw format) apply to the generated isopach maps, Figure 6.5 shows profile J0820250LK, as well as the six top-most isopach maps. A yellow circle shows where the profile is located. For further orientation, a topographic map is also provided. This map shows the location of the boundary polygon in relation to the field area. The interpretation of the data represented in Chapter 3 is also shown, giving an indication of how the axial zones and margins of the lobes fit in relation to the isopach maps.

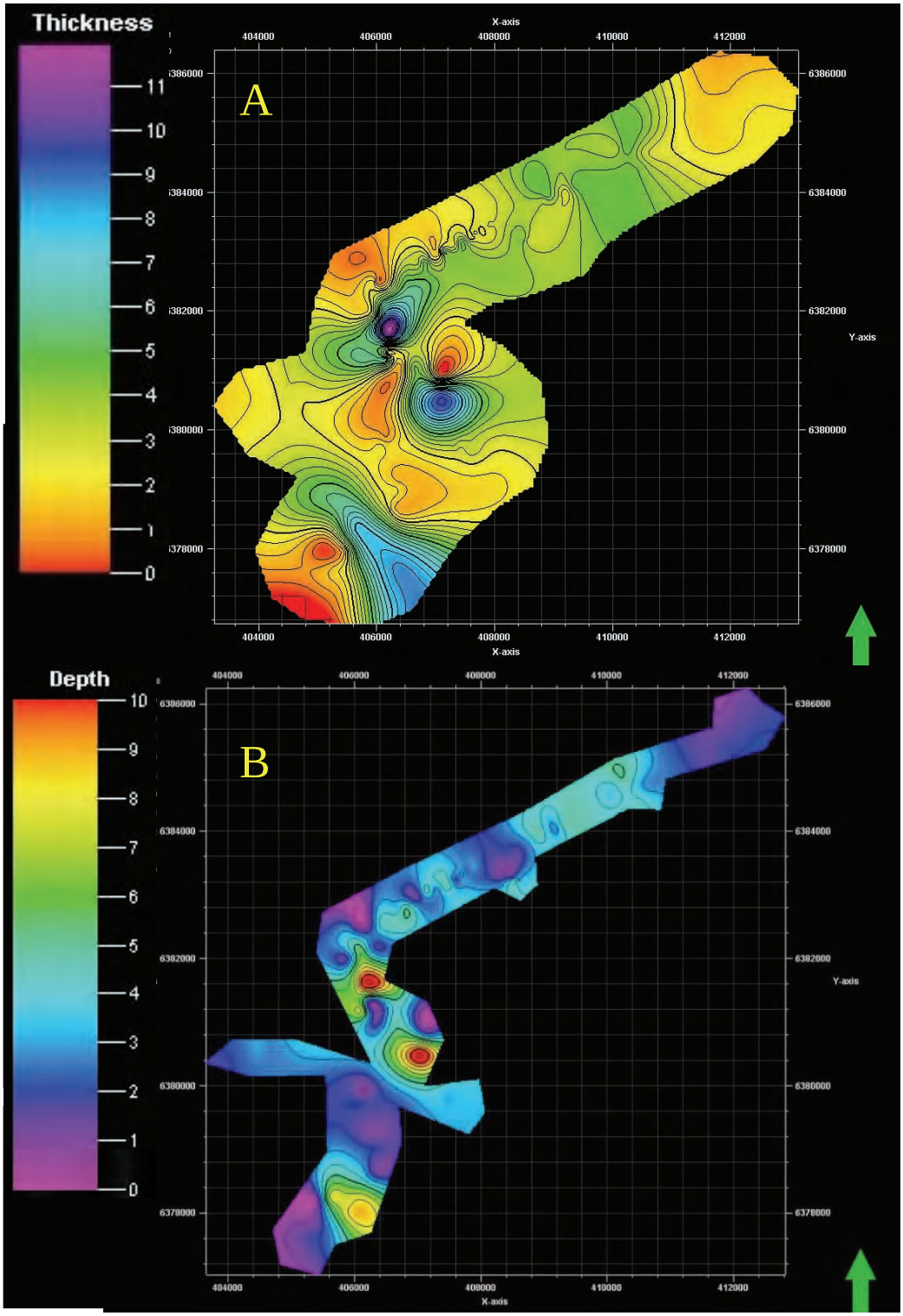

Figure 6.4 Example of the difference between the first isopach maps and the final product. Both represent Lower Lobe 5. (A) used the old, larger polygon, and the colour scales were automatically adjusted to the minimum and maximum values. (B) used the constrained polygon and the colour scale was manually set to 10 metres. The results may appear similar, but there are some significant differences: (B) has a much smaller degree of contouring. The purple in (B) is both a result of outcrop not revealing the whole of the lobe (in the west and south), as well as true thinning (east).

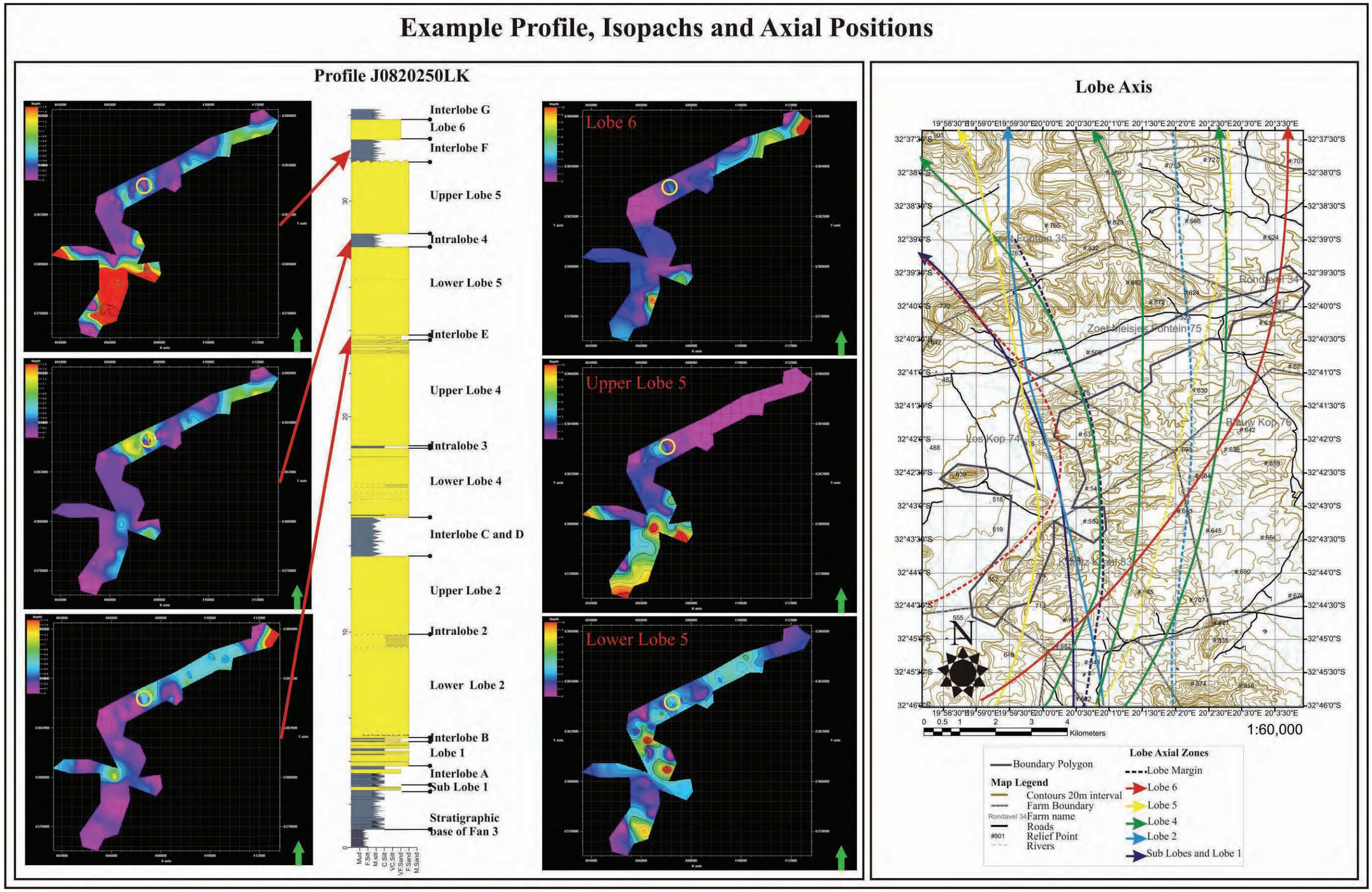

Figure 6.5 Example of isopach maps in relation to a vertical profile, as well as the axial positions of all lobes, determined from the isopach maps and field data (Chapter 3). Also provided on the axis map is the location of the boundary polygon in order to gain perspective on the location of the isopach maps. The yellow circles on the isopach maps represent the location of the example profile.

6.4 Discussion

6.4.1 Lobe formation

An initial aim of the Lobe project, in terms of the deposition of Fan 3, was to create a single model to represent the whole fan. The features mentioned above should already show the difficulty with such an approach. The complexity of Fan 3, even on a lobe-element scale, makes a single model difficult, if not impossible. Rather, it would seem that a different depositional model should be constrained for each individual lobe, or even lobe-element.

A basic pattern that can be established is an inferred gradual basin-ward stepping of the lobes and lobe-elements, followed by back-stepping of the last lobes. The oldest lobes (the sub-lobes) never reach the northern outcrop, whereas Lobe 1 only just reaches that far. The younger lobes all pinch-out slightly to the north of the lobes that developed earlier, with Lobe 4 being the last to pinch-out north of Klip Fontein (Prélat *et al*., in review). Lobe 6 pinches out earlier (back stepping). The northern pinch-out of Upper Lobe 5 is unknown, as its separation from Lower Lobe 5 was not observed by Prélat *et al*. (in review).

The progradation-aggradation-retrogradation pattern described in Chapter 4 can also be attributed in part to the basin-ward stepping pattern. A basin-ward stepping could mean several things, including a basin-ward shift of the source area, or a decrease of accommodation space (relative sea-level fall). This would cause the “mid-sections” of the lobes, which are associated with the mid-fan area, to also shift north. Therefore, in a strike-section the appearance would be that of the progradation-aggradation-retrogradation pattern as described above. A likely scenario here was probably a combination of both, namely a minor influence from allogenic controls, and a major contribution form autogenic controls. Allogenic controls influence the sediment supply into the basin and the distance a lobe can deposit into the basin. Autogenic controls influence the lateral extent of a lobe, and the direction of deposition (lobe switching and stacking, influenced by basin-floor topography and the presence of pre-existing lobes).

No channels (as described by Johnson *et al*., 2001) are present in the study area, therefore the transition from channel to sheet deposits cannot be examined. However, the transition from a single axial zone deposit to deposits with multiple axial zones can be inferred. This can be

accomplished by using Upper Lobe 5 and Lobe 6 as single axial zone analogies, and Lobes 2, 4 and Lower Lobe 5 as multiple axial zone analogies.

Single axial zones are the mid-fan continuations of channels which are mostly restricted to more proximal locations. A general appearance is an area of focussed flow, characterised by

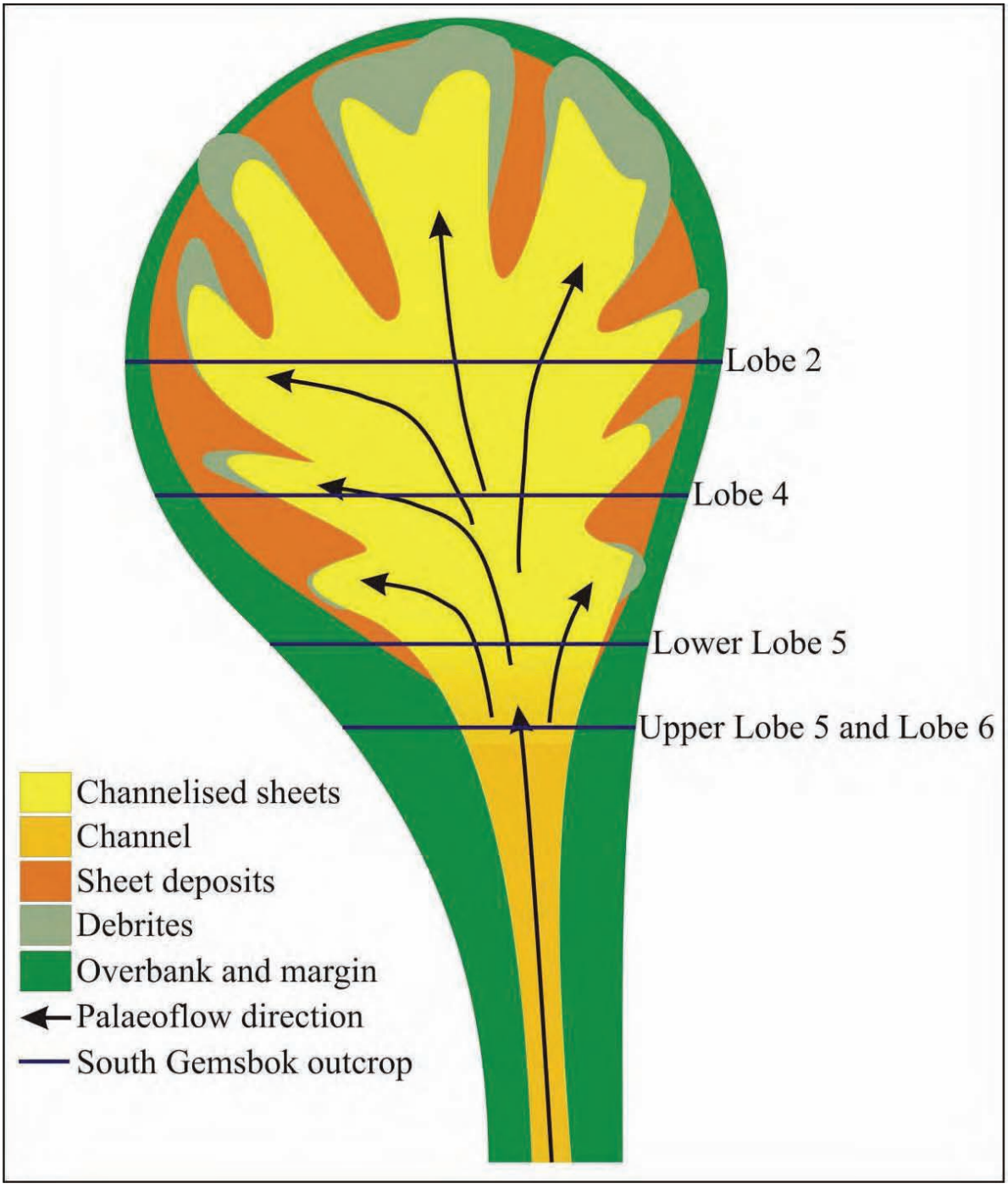

Figure 6.6 Schematic of the structure of a lobe. The diagram illustrates the transition from channel to channelised sheets, and channelised sheets to sheets. The single axial zone is the transition zone from confined flow to unconfined floor spreading. Also indicated is the position of the southern Gemsbok Valley outcrop in relation to Lobes 2, 4, 5 and 6.

heavy amalgamation and minor scouring at the base, rapidly becoming more structured in a lateral direction, with bedding planes and depositional features becoming more prominent.

When these features reach the basin floor or leave confinement, they become distributive. The exact direction of distribution can be dependant on basin-floor topography, palaeoflow direction, flow strength and sediment load. Successions of flows will distribute in various directions, stacking to form multiple axial zones. Areas with multiple axial zones display similar features to a single axial zone, namely large amalgamated sections with minimal scouring at the base, becoming more structured laterally. A distinguishing feature is present towards the margins, namely the finger-shaped deposits, as well as the probable presence of debrites. Haughton *et al*. (2003) referred to these co-genetic debrites as "linked-debrites" in order to emphasise their connection to precursor sandstone beds. Talling *et al*. (2004) identified this co-genetic debrite-turbidite feature in the Miocene Marnoso Arenacea Formation in the Italian Apennines, the Silurian Aberystwyth Grits in Wales and Quaternary deposits of the Agadir Basin, offshore Morocco.

Prélat *et al*. (in review) described the nature of the thin-bedded intervals as possibly linked to allogenic and autogenic controls. In the case of autogenic control, the thin-bedded intervals are the marginal continuations of lobes that thicken towards the centre. In the case of allogenic controls, the thin-bedded intervals represent a reduction in sediment supply to the system. It has already been indicated that allogenic and autogenic processes interact (Stouthamer and Berendsen, 2007). Prélat *et al*. (in review) indicated that the interlobe intervals of Fan 3 fine and thin in a down-dip direction, and do not grade laterally into sandstone. In the study area for this project, the fine-grained intervals also do not alter lithofacies into sandstone, however, they show an up-dip thickening and some are interbedded by thin-bedded sandstones up-dip. This could indicate a possible interaction of allogenic and autogenic process, as the possibility exists that some of the fine-grained intervals are related to smaller, low-volume deposits, whereas the rest clearly represent a reduced sediment supply.

Figure 6.6 is a diagram of the features described above, as well as the locations of transition zones from channels to channelised sheets (structureless sandstone dominant), and channelised sheets to sheet deposits (structured sandstone dominant). In the case of finger-shaped lobes, sheet deposits are present only between the channelised sheets of the axial zones. Figure 6.6 also indicates the location of the south Gemsbok River valley outcrop in relation to the basic lobe

shape. Note that there are no “hard lines” separating the zones. The reason for this is that the transitions are often not abrupt, and grading between them is common.

6.4.1 Lobe stacking

Topography can have a major influence on the flow direction of sediment gravity flows, ranging from diverting to complete damming of flows (Kneller and Buckee, 2004; Prather *et al*., 1999; Pickering *et al*., 1989). Topography can constitute a basin floor feature, or result from the presence of a previous deposit. In a distributive system, a deposit from a single flow has the appearance of a thickened “mid-section”, the equivalent of a channel, with thinning sheet deposits moving away from the centre. The channelised area would constitute a topographic high, and the sheet deposits topographic lows. Basic physics dictates that a flow should follow the path of least resistance. A new flow would therefore divert around the obstacle. The exact behaviour of a turbidity current in such a situation depends on the forward velocity of the flow, the height of the topographic obstruction, the density of the flow, and the density stratification of the flow (Alexander and Morris, 1994; Lane-Serff *et al*., 1995). The result of such behaviour would appear in a strike section as laterally or vertically stacked flows, or a combination of stacking patterns.

The mid-fan strike section stacking pattern of all the lobes is shown in Figure 6.7. Note that this diagram is not to scale, and that anything to the right of the red line is unknown (the line represents the western end of the Gemsbok River valley outcrop). The lobes of mid Fan 3 show a

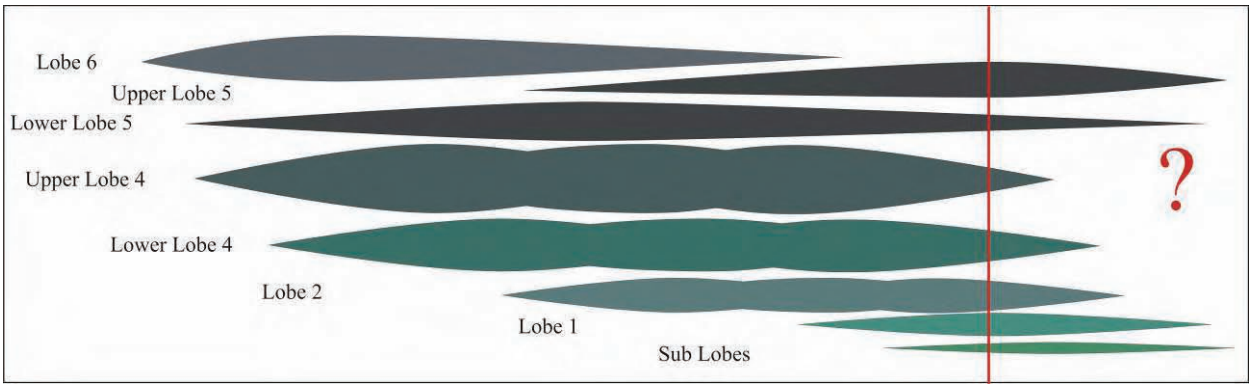

Figure 6.7 Schematic to illustrate the strike section stacking pattern of Fan 3 in the mid-fan area (southern Gemsbok River valley) The red line represents the western end of outcrop in the valley. Not to scale.

combination of compensational lateral and vertical stacking patterns of channelised zones. Pure stacking involves the erosion of previous sandstone deposits, whereas compensational stacking does not necessarily involve erosion of previous sandstone deposits. The lobes stack without major scouring or erosion of sandstone units. Interbedded siltstones are, however, eroded away, amalgamating sandstone units together.

As an example of the basin-ward stepping of the lobes, Figure 6.8 illustrates the relative positions of the Lobes in relation to each other. The arrows represent the stepping pattern, black showing progradation (basinward stepping), red showing aggradation, and yellow showing retrogradation (back stepping). Prélat *et al*. (in review) provides a more detailed description of the outcrops to the north, including more detailed margins for the lobes. Note that the figure does not show the individual upper and lower units of Lobes 2, 4 and 5. The reason for this is that Prélat *et al*. (in review) did not distinguish these units to the north, therefore their distribution in the northern outcrop is not known.

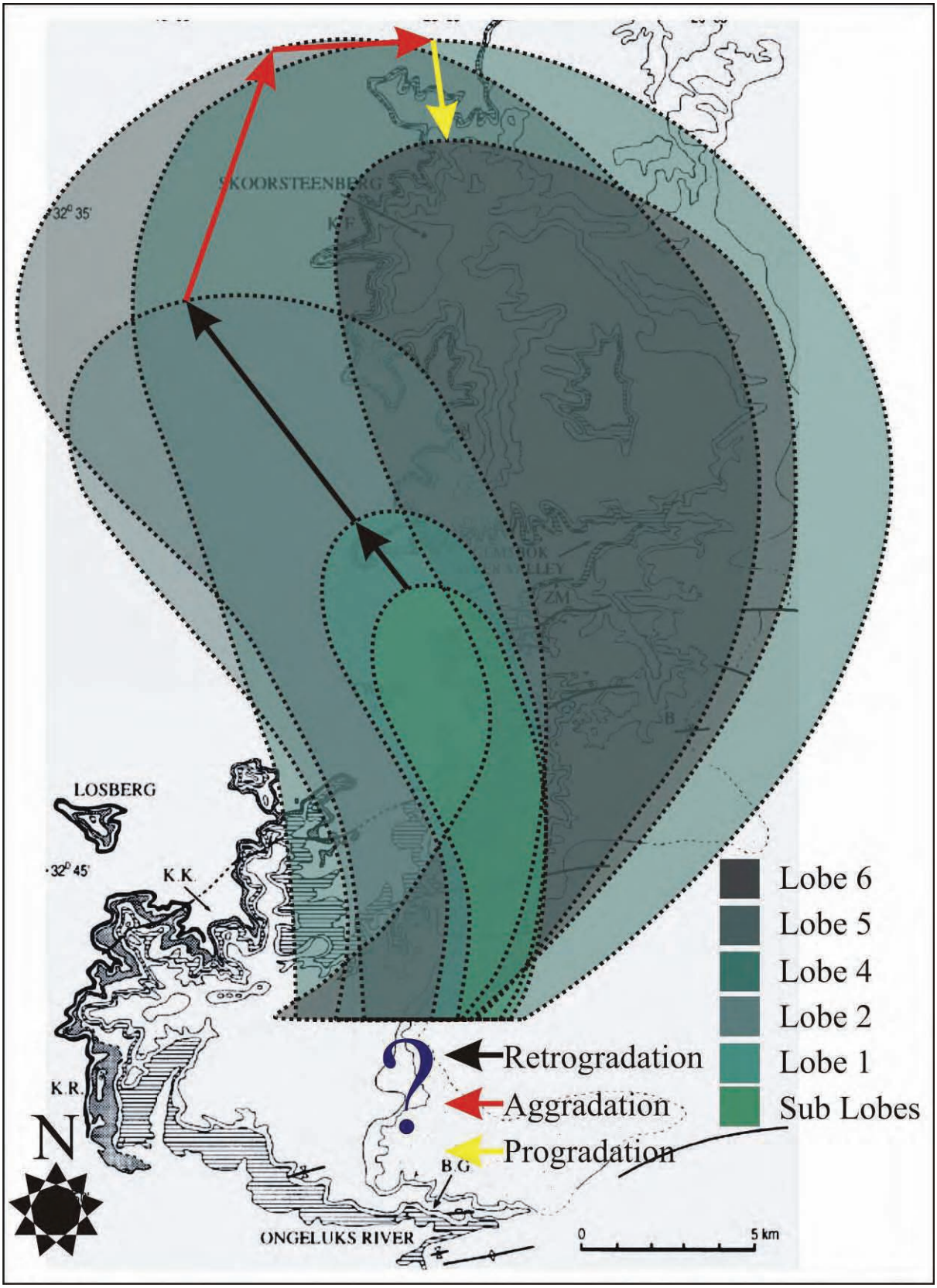

Figure 6.8 Schematic of the probable locations of the Lobes in order to illustrate their positions relative to each other. Also shown is the inferred stepping pattern for the lobes. The black arrows represent basinward stepping (progradation), the yellow arrows represent aggradation, and the red arrows represent back stepping.

Chapter 7

Data Modelling in Petrel

Data Modelling with Petrel

7.1 Introduction

The importance of turbidity flow deposits as hydrocarbon reservoirs has resulted in a massive increase in exploration and research being conducted on these features (Pyrcz *et al*., 2005; Stow and Mayall, 2000). This research focuses particularly on the internal and external architecture, as well as the stacking patterns of elements (Shanmugam, 2000; Stow and Mayall, 2000; Johnson *et al*., 2001). Stochastic models provide a method of modelling the response of a reservoir to lithofacies, porosity and permeability. Static models provide 3D representations at a fixed point in time, be it from a working model, or real data from outcrop and subsurface imaging, and are good for viewing a potential reservoir in 3D. Advances in modern computer technologies mean that computer based realisations can be constructed faster and in much greater detail. Pyrcz *et al*. (2005) indicated that the two main methods used for the construction of stochastic models are object-based Boolean techniques, introduced by Haldorsen and Lake (1984) and Haldorsen and Chang (1986), and surface-based techniques, introduced by Deutsch *et al*. (2001) and Pyrcz and Deutsch (2003). The surface-based model requires that the general geometry of lobes and lobe-elements (or flow events as used by Pyrcz *et al*., 2005) be known or, at the very least, constrained before modelling begins. Other attributes, such as grain-size distribution, source location, bathymetry, flow path and the characteristics of lobe geometries, are also important (Pyrcz and Deutsch, 2003).

Large amounts of data were gathered during the fieldwork for this project. However, a problem which is immediately evident is the linearity of outcrop in the study area. For three-dimensional realisations to be realistic, decent 3D constraint is critical. This chapter shall attempt to determine if the data gathered can be used effectively in the production of 3D models. This shall be done by seeing how many steps of model building can be performed.

The manipulation of the data gathered during fieldwork was completed following several steps in a defined workflow:

- Digitisation of data through the use of programs such as DSL, CorelDraw X3 and Microsoft Excel 2003, proving several different uses for the same data (Chapter 5)
- Import into and manipulated with Schlumberger's Petrel, version 2007.1.2.

- Isopach map building (Chapter 6)
- Surface creation
- Static model grid building
- Lithofacies distribution modelling

This chapter will focus on several aspects of the modelling process. First the data will be discussed, providing examples of all the different forms used. Then the modelling process with Petrel will be discussed in detail, as well as the methods used and the limitations encountered. Lastly the results of these manipulations shall be discussed.

7.2 Petrel Modelling

Schlumberger's Petrel is a powerful software package capable of modelling most aspects of a petroleum reservoir. It includes a myriad of algorithms developed to create visual representations of complex physical features in 3D. For this project, only a small part of the program's capabilities was exploited, namely the grid building and facies modelling features and the ability to create isopach (thickness) maps. The aim here was to create a 3D representation of the conceptual depositional model (Chapter 6). For a short description of some of the algorithms

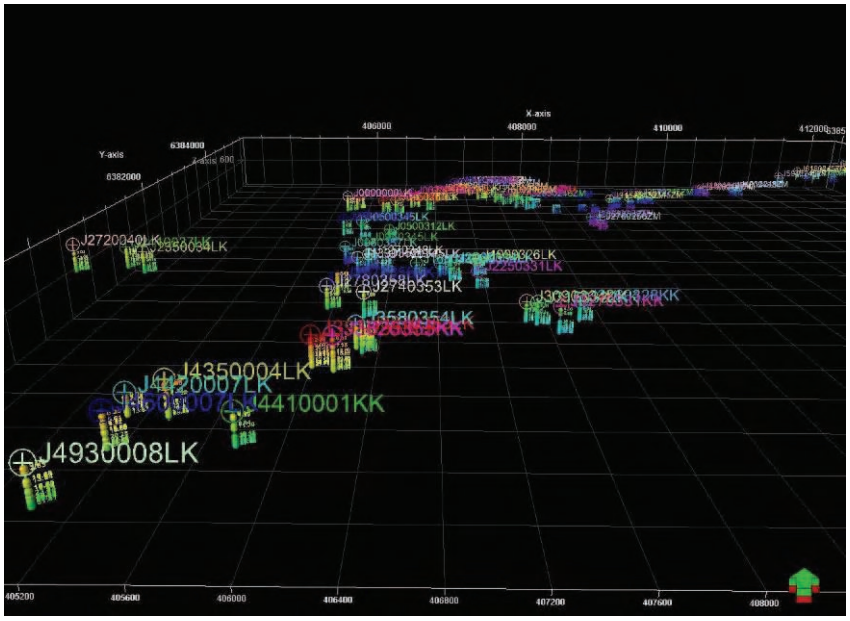

Figure 7.1 A 3D view in Petrel, looking north, of the wells and well-tops used. These data represent all 72 vertical profiles (wells).

used by Petrel to create the features, based on Petrel's Online Help files, please refer to Appendix E.

7.2.1 Field size

Figure 7.1 is a view from the south, showing the entire study area. Both the wells and their associated well tops are shown. The entire study area covers an area of almost 10 kilometres from east to west, and about 7 kilometres from north to south. The entire area could not be included as is for the initial modelling attempts. The layout and positions of lobes and lobe-

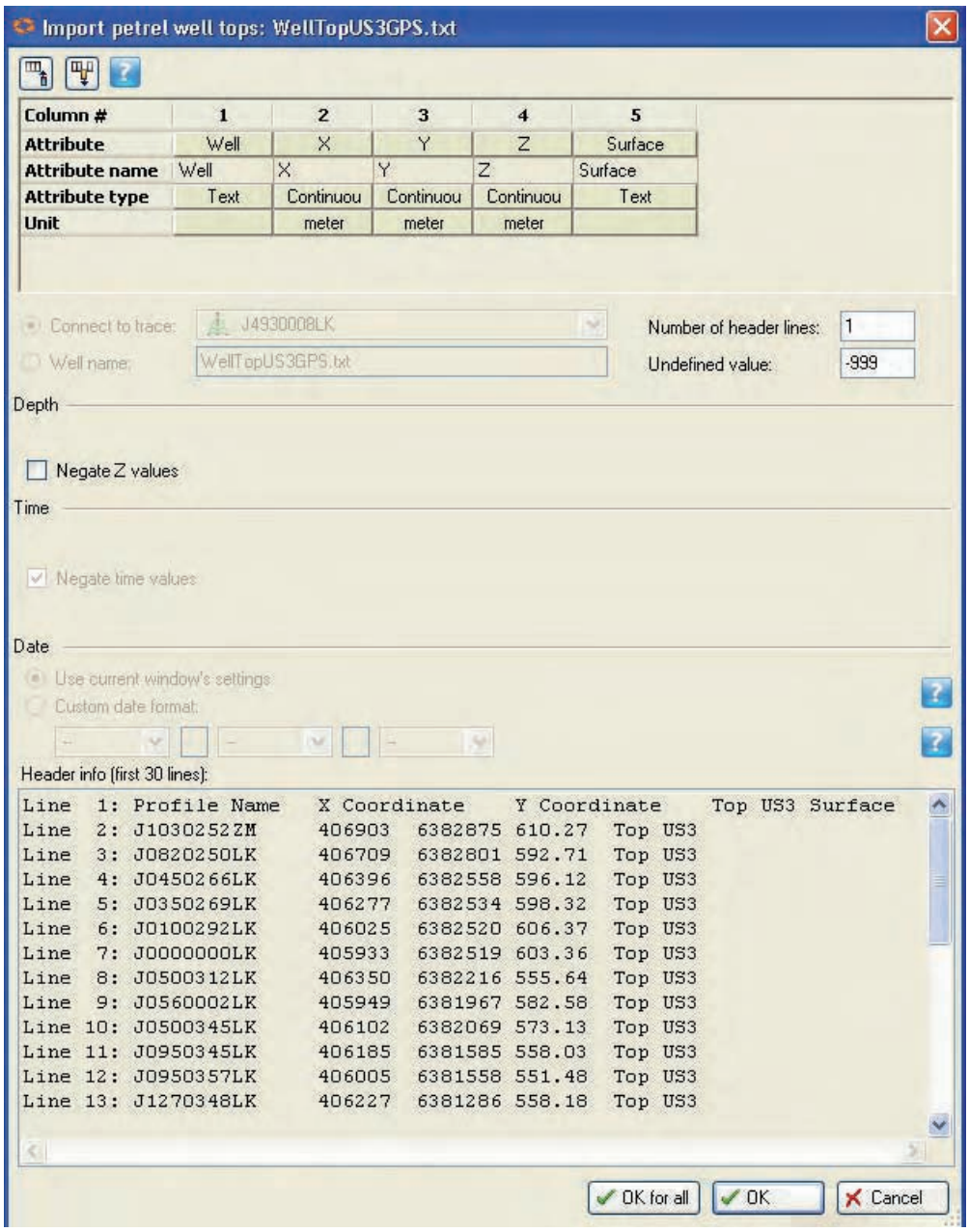

Figure 7.2 Example window of how data appear when imported from text files into Petrel.

elements, as well as the known pinch-outs, were discussed in previous chapters, and the problems with modelling this will become clear later. Of the 72 wells available to Petrel, only the Loskop wells were used for the initial modelling, i.e. less than half of the total number of wells. All wells were used for surface and thickness map creation, as well as for the last attempted modelling.

7.2.2 Logs and correlation

The DSL wells were imported into Petrel as iRap RMS well logs. With this method, the bed thicknesses, grain-sizes and lithofacies where all imported simultaneously for all the wells. It is also from this that the x-, y-, and z-coordinates for each well are read, the latter being the northing and easting data measured with handheld GPS receivers. Petrel uses the top z-coordinate as the Kelly Bushing (KB) height (effectively the height of the drilling platform), unless instructed otherwise by the user. Because of this, all wells are imported at the correct topographic height, or at least as accurate as the GPS equipment allowed.

The above mentioned import method does not include the tops and bases of individual lobes. For this reason the Excel spreadsheets were sorted and exported as text files. These data are then imported as well tops, which automatically link to wells. Fig. 7.2 is an example of such an import window. All required data have now been included, namely both well logs and their correlations in the form of well tops (at least for the individual lobes).

7.2.3 Surfaces

Most, if not all, of the algorithms mentioned in Appendix E can be used to create 3D surfaces in Petrel, varying in accuracy to a greater or lesser degree depending on the type and quality of the data used. Due to lack of experience and sufficient understanding, only two of these were used. A boundary polygon (line) can be used in all cases to constrain the amount of extrapolation the program performs. This is not strictly necessary, but if the algorithms are left to extrapolate past a certain distance from the data points (usually only a few hundred metres), the results can no longer be trusted to be accurate or realistic. This is of course dependent on the spread of the data.

For the first few attempts, five different polygons were used, since not all of the lobes are present everywhere. This created problems when the surfaces were adjusted for overlap. When Petrel creates a surface, it has to extrapolate the data. Commonly this creates a situation where two surfaces overlap, which geologically cannot happen, especially if the two surfaces are the top and base of a single unit. For this reason, the surfaces first have to be adjusted again. A simple function allows Petrel to set the Z-values of the bottom surface equal to that of the top surface (or visa versa) when the bottom Z-value is equal to or greater than the Z-value of the top surface. Here the first problem with multiple polygons emerges: this calculation can only be done for units with the same polygon, otherwise all the surfaces will be cut to the shape of the top-most surface, resulting in a loss of information for the isopach maps and 3D grid. This same problem applies to the siltstone units situated between sandstones. Unless they are within a lobe or lobe-element, and only if the sandstone units do not pinch-out (in which case the siltstone units “merge”), they cannot be accurately represented in isopach maps. Later attempts worked better after the spreadsheets were adjusted to use a single boundary polygon. The default grid size of 50x50 metres was initially used, but was later reduced to 20x20 for better resolution. Figure 7.3 shows the six different polygons used during the Petrel runs. Note the much reduced size of the constrained polygon.

The Kriging Interpolation algorithm was used first. Most variables were left at their default values. The only aspect manually adjusted was the range, which was set at 2000 (metres) for both major and minor direction. The result was a set of surfaces that showed a great deal of contouring, but had trouble honouring the well data, in other words the surfaces were too smooth. For testing purposes, the range was set to 6000. The result was an even smoother surface which fitted the data even less. Fig. 7.4 A. shows an example surface for this method at 10 times vertical exaggeration. Note the smooth surface contours. This smoothing effect is an example of the effect well influence radius has on the resulting trends, and can be resolved by reducing the influence radius.

The trends used by the algorithms are heavily influenced by topography and distances between data points (wells). The algorithms function along a trend around a well. If a well’s influence radius extends past another well, the algorithm has to average out the trend, but does not necessarily adjust correctly to the new well. The result is a smoothed surface that does not honour the data.

While the Kriging algorithm is useful, the nature of the input data from this study makes it difficult for the algorithm to function properly (according to Petrel's Online Help files). For this reason, the Convergent Interpolation algorithm, which is the default algorithm, was used to form the surfaces used in building the grid for modelling. This algorithm was far more accurate in keeping to the data (Fig. 7.4 B). To make it even more accurate, a "well adjustment" was completed by adding the well tops as a constraint. The result was a surface that made contact with all the data points, even though it had a bit of a bulleted appearance (most detail centred around wells).

In order to illustrate the problem with the Kriging algorithm with this data-set, Appendix D

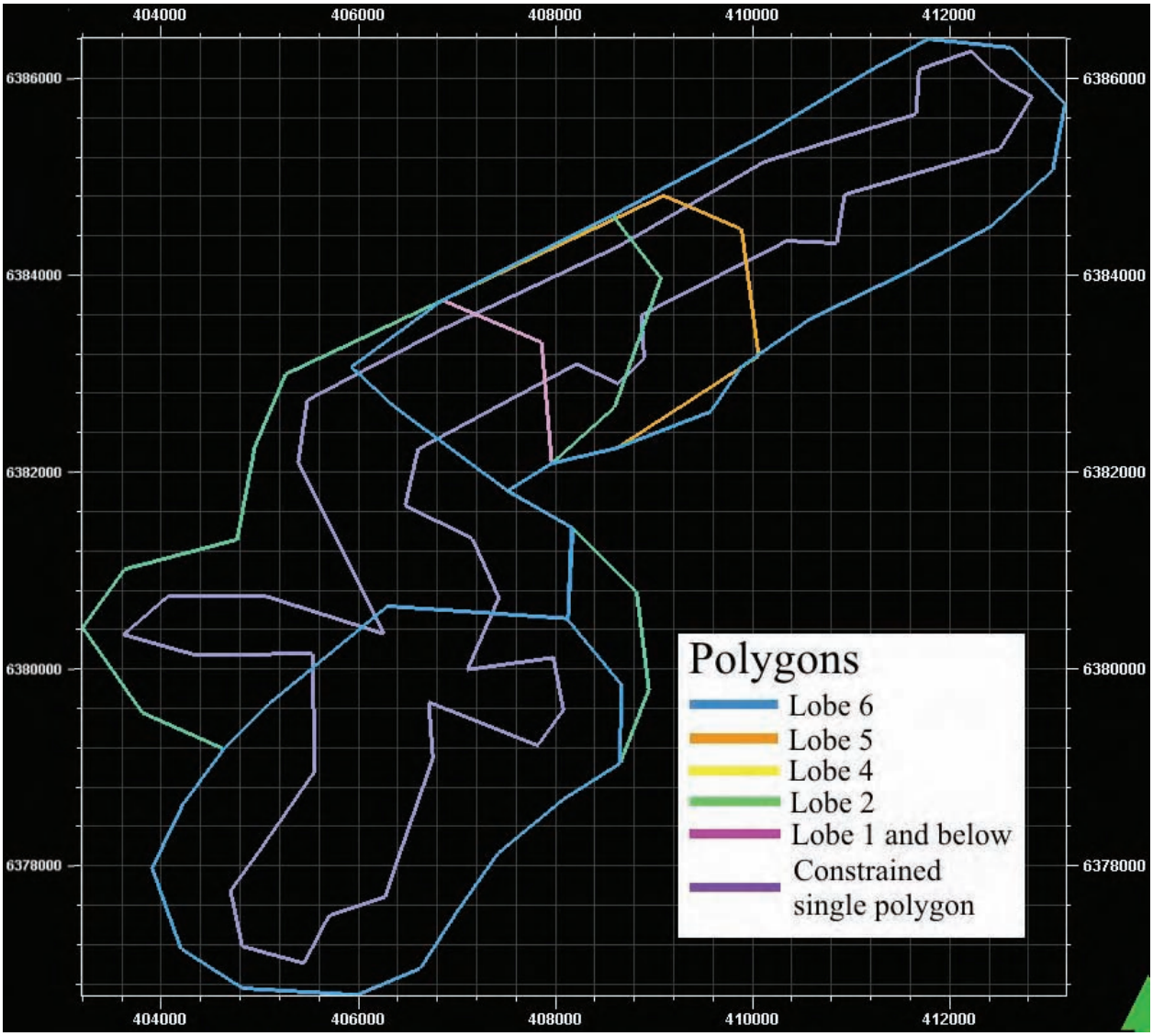

Figure 7.3 The different polygons used in various runs in Petrel. The constrained polygon was used for the final product.

displays two versions of Figure D.1. The first panel contains both the accurate well-tops, as well as the surfaces created using the Kriging algorithm (See Chapter 7 and Appendix E), whereas the second only contains the well-tops (for a clear view). These are provided in order to illustrate the inaccuracy of the Kriging algorithm with the data for this study. Note that Fig. D.1 and D.2 use the original data, before the adjustments were made. The Kriging method resulted in the loss of much data, as the surfaces cut away much of the tops and bases of the wells. In some cases, the wells were reduced to less than a metre in length.

The final runs in Petrel used the newly adjusted spreadsheets, allowing the use of only a single polygon. This last polygon was also constrained more around the data points, leaving less room for the algorithms to extrapolate. The Convergent Interpolation algorithm was again used as above, but the grid size was changed to 20x20 metres, making it even more accurate.

Figure 7.4 shows the surfaces created for upper unit 2 using both Kriging (2000x2000 direction) and convergent interpolation. From this the difference between the two methods is clear: Kriging makes far bolder extrapolations, resulting in much exaggerated topography. Both are at 10 times vertical exaggeration.

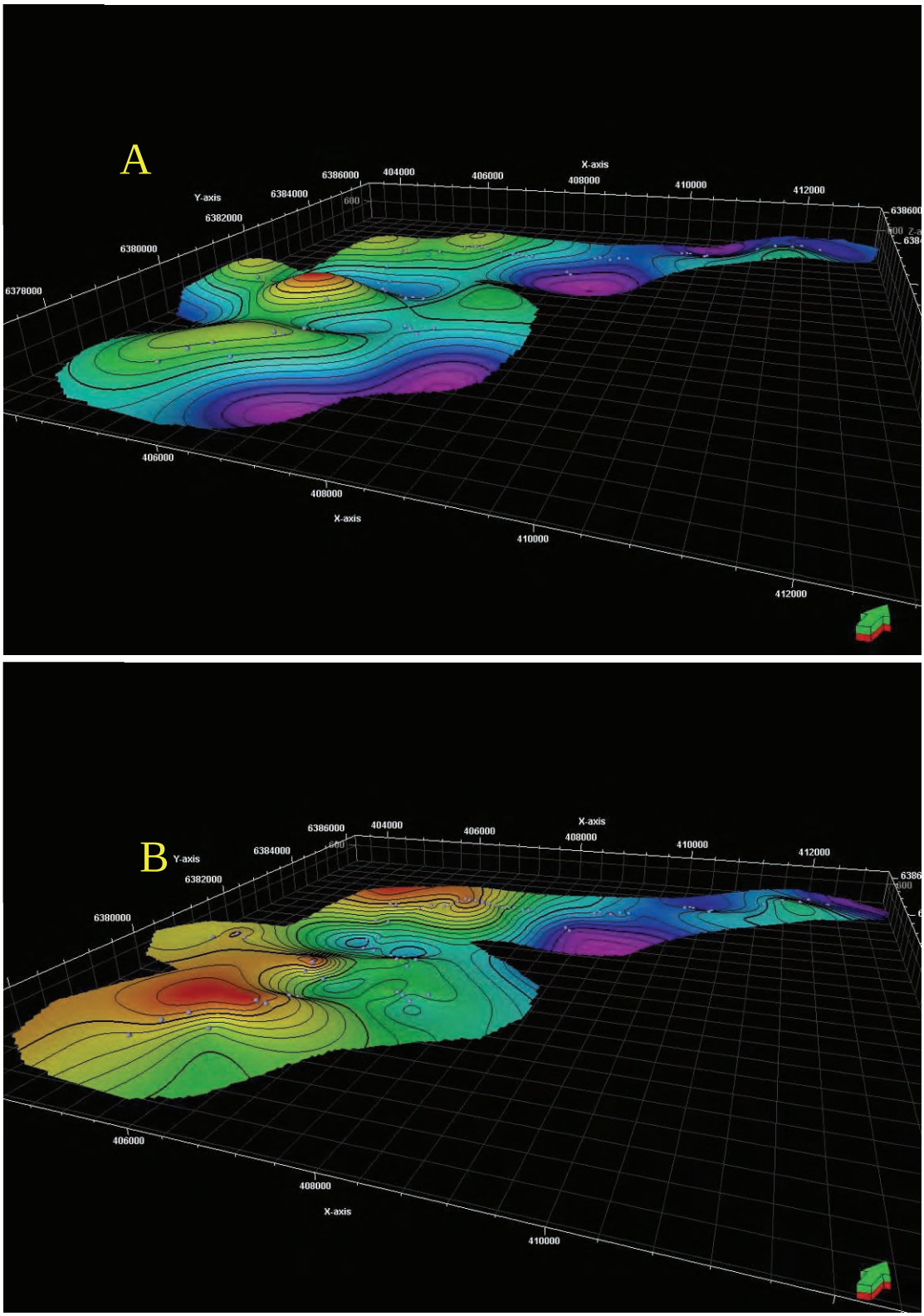

Figure 7.4 Two of the initial surfaces created in Petrel. (A) used the Kriging algorithm, whereas the Convergent Interpolation (CI) algorithm was used for (B). Note the difference in surface shape between the two methods: Kriging created a much smoother surface but was unable to keep to the data, whereas CI managed to honour the data points to an acceptable degree.

7.2.4 Grids, Zones and Layering

Grids, zones, and layering are key features used to define a model. A grid is defined by using the surfaces created above (after Z adjustments), and providing the x and y dimensions for each cell. In this case, the dimensions were set to 20 metres a side. Because of computational constraints, the cells could not be any smaller. They need not be smaller for this model, as all wells are located far enough apart that a grid of 20x20 metres would place each well in its own cell (wells should not share a cell). The second problem with the original data arises here: all the data were used for the grid, but only a part of the western part of the field area was used, as this is the only place where all 5 boundary polygons overlap. Thus the grid was much smaller than intended.

The grid is defined in the z-axis by zones, the Petrel analogue for architectural elements such as lobes. They were built by using the “conformable” command, which forces them to follow the correlated well tops. Fig. 7.5 is an example of these zones as created in the initial runs.

Layering can be seen as the z-dimension of the cells. For the first few attempts it was set to 20 centimetres, and layered using the “Follow-top” command, which sets the cell layering parallel to the top of the zone. The choice between “follow top” and “follow base” was based on the fact that all the data used were based on the top z-value for each well, but refer to whether a unit should show top-lap or down-lap. Again the layering thickness was limited by the computer’s processing ability. This layering will also be used to up-scale (block) the lithofacies from the well-logs. The thickness of the layers determines whether a field measured feature will be visible or not. The DSL logs included all measured layers, but a too low resolution during layering in Petrel will average out these layers, resulting in a loss of data.

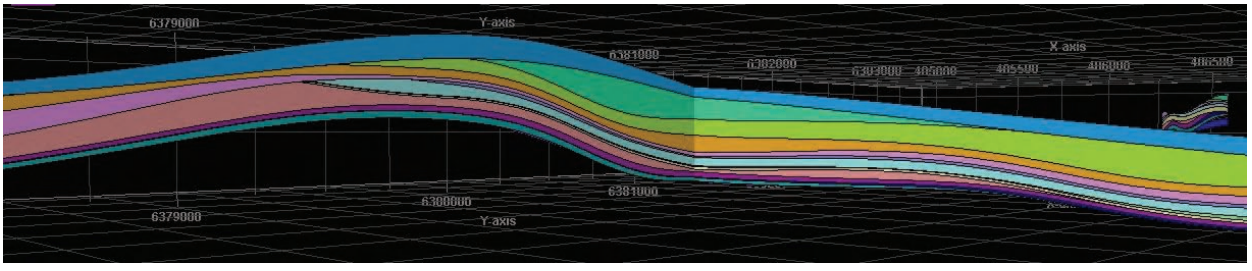

Figure 7.5 This figure shows the zones created in the first grid run. The surfaces created from the larger polygons caused some major pinch-out features when grouped together. One of the reasons for this is because they used different polygons, and as such the Z values could not be correctly adjusted.

After the data were adjusted for a single boundary, the layer thickness in the cells could no longer be set to a fixed value, as the computer could not handle such detail. Instead, the layering was set to proportional. Sand-prone zones were given 60 layers, whereas silt-prone zones were given 10.

7.2.5 Facies modelling

Up-scaling is the process of expanding a 1D well log into the 3D area of its grid cell. When up-scaling, or "blocking", wells for facies modelling purposes, the layering thickness is important. If the thickness is set too high, thin units will be cut out, and will thus not be included in the model. At 20 centimetres, the major siltstone breaks are mostly preserved for this study, but not completely (Fig. 7.6 A). Initially it was felt that the silt-prone zones should be given only a single layer and a fixed colour in order to better display them. However, as Panel 12 in Chapter 3 indicates, these silt-prone units start to become more sand-prone down-dip. In order to represent this, these zones were also given layering, albeit less than the sandstone prone zones.

The facies modelling was based on the up-scaled well-logs mentioned above. All 17 lithofacies types from DSL were included, though only a few were used. Up-scaling is dependent on several factors, namely the 1D lithofacies, layering thickness, and the surface geometry of the zones.

The facies modelling was first attempted by using the Indicator Kriging algorithm. The method is useful in that the results are directly repeatable and it avoids over-interpretation of the data. However, the data were not suitable for this method, as the resulting facies model lacked enough detail (Fig. 7.8 A).

The second method used was Sequential Gaussian Indicator Simulation. This is a useful method when the exact shape of lithofacies bodies is uncertain. This algorithm turned out to be the best choice as it included a lot more detail.

Figures 7.8 and 7.9 are the results of the first two simulation runs. Fig. 7.8 was constructed using the Kriging method and it shows a lot less detail than the facies model in Fig. 7.13, which used the Sequential Gaussian indicator method. Cross-sections (blue surfaces) were made to illustrate the difference in 2D. The difference is just as prominent here.

The final run used the adjusted data. It could therefore include the whole field area. In order to better match field observations, and to create a less cluttered model, DSL's 17 lithofacies were reduced to only 5 by grouping similar lithofacies. This was done in Petrel by using the calculator function, basically telling the program to make a specific x value equal to a new y value. The result of this process is shown in Table 7.1 and Figure 7.6. The new colours are also shown for the reduced lithofacies. The final facies model is shown in Figure 7.9, and its two cross-sections in Figure 7.10. These cross-sections correspond to Panels 3 and 12 in Chapter 3.

The accuracy of the facies modelling process can be shown by a simple histogram. Fig. 7.7 displays the results for the final facies modelling run. The percentage of a lithofacies present is shown on the y-axis, and the lithofacies are listed on the x-axis. The red column represents the original 1D lithofacies as provided by the well logs (reduced from the DSL lithofacies); the green represents the lithofacies proportions after up-scaling (the blocked wells); and the blue logs are the proportions (in 3D) after the lithofacies have been modelled in 3D. The aim is for the 3D model lithofacies to honour the 1D input data in 3D. The results, however, show a decrease in structureless sandstone and a proportional increase in structured sandstone.

The final facies model is shown in Figure 7.10, with the corresponding cross-sections in Figure 7.11. This final model is good enough to be comparable to the corresponding correlation panels in Chapter 3. Note that the correlation panels in Chapter 3 are not linear features (Fig. 3.14), whereas the cross-sections in Figure 7.11 are.

DSL Lithofacies	Reduced Lithofacies	Chapter 3 Lithofacies
Background	Background	Hemipelagic Suspension Deposits
Mudstone		
Mudstone / Siltstone (>50%)		
Siltstone / Mudstone (>50%)	Siltstone	Parallel- and ripple-cross-laminated siltstone
Laminated / Rippled Siltstone		
Siltstone / Sandstone (>50%)		
Sandstone / Siltstone (>50%)	Structured Sandstone	Structured Sandstone
Laminated / Rippled Sandstone		
Climbing Ripple Lam. Sandstone		
Structured Sandstone		
Structureless Sandstone (Sheet)	Structureless Sandstone	Structureless Sandstone
Structureless Sandstone (Channel)		
Channel Lag (Mud-clast conglomerate)	MCC	Mud-Clast Conglomerate
Channel Lag (Sand-clast conglomerate)		
Slump (sandstone)		
Slump (Mud)		
Debrite		

Table 7.1 Summary table of the lithofacies used. The DSL lithofacies were grouped in order to better match the lithofacies descriptions as given in Chapter 3.

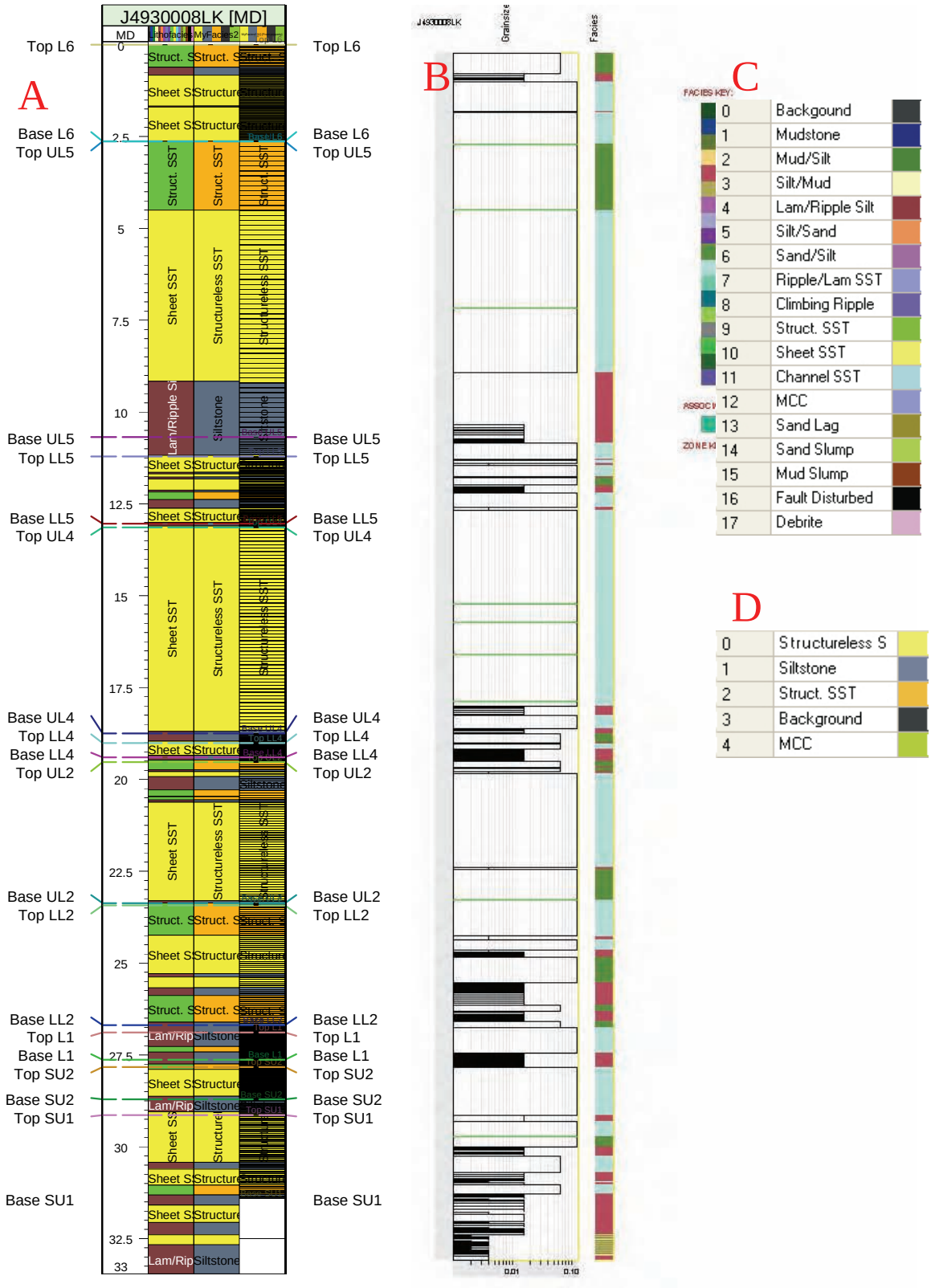

Figure 7.6 Well J4930008LK. The detailed representation (A) is from Petrel. It shows both lithofacies lists used, namely the DSL lithofacies in the left column (lithofacies group C) and the reduced lithofacies in the middle column (lithofacies group D). The column to the right shows the result of proportional layering. The DSL profile (B) is again provided as a comparison.

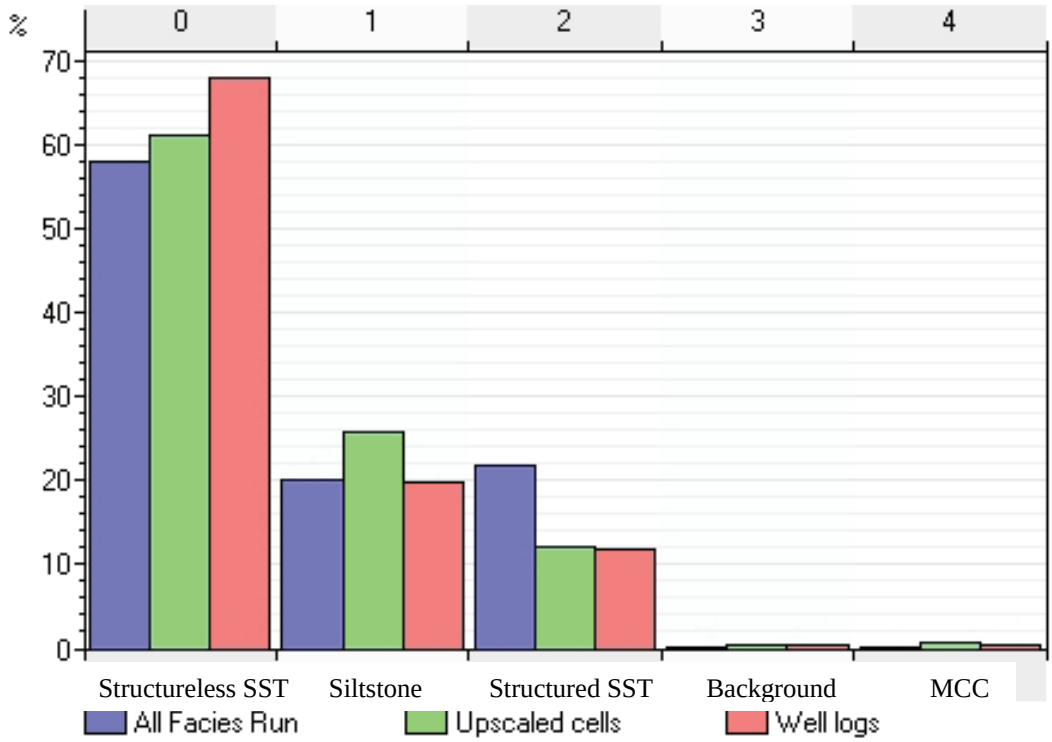

Figure 7.7 The proportion of lithofacies present before and after lithofacies modelling. The percentage of a lithofacies present is shown on the y-axis, and the lithofacies are listed on the x-axis. The red column represents the original 1D lithofacies as provided by the well logs (reduced from the DSL lithofacies); the green represents the lithofacies proportions after up-scaling (the blocked wells); and the blue logs are the proportions (in 3D) after the lithofacies have been modelled in 3D. The aim is for the 3D model lithofacies to honour the 1D input data in 3D. The results, however, show a decrease in structureless sandstone and a proportional increase in structured sandstone.

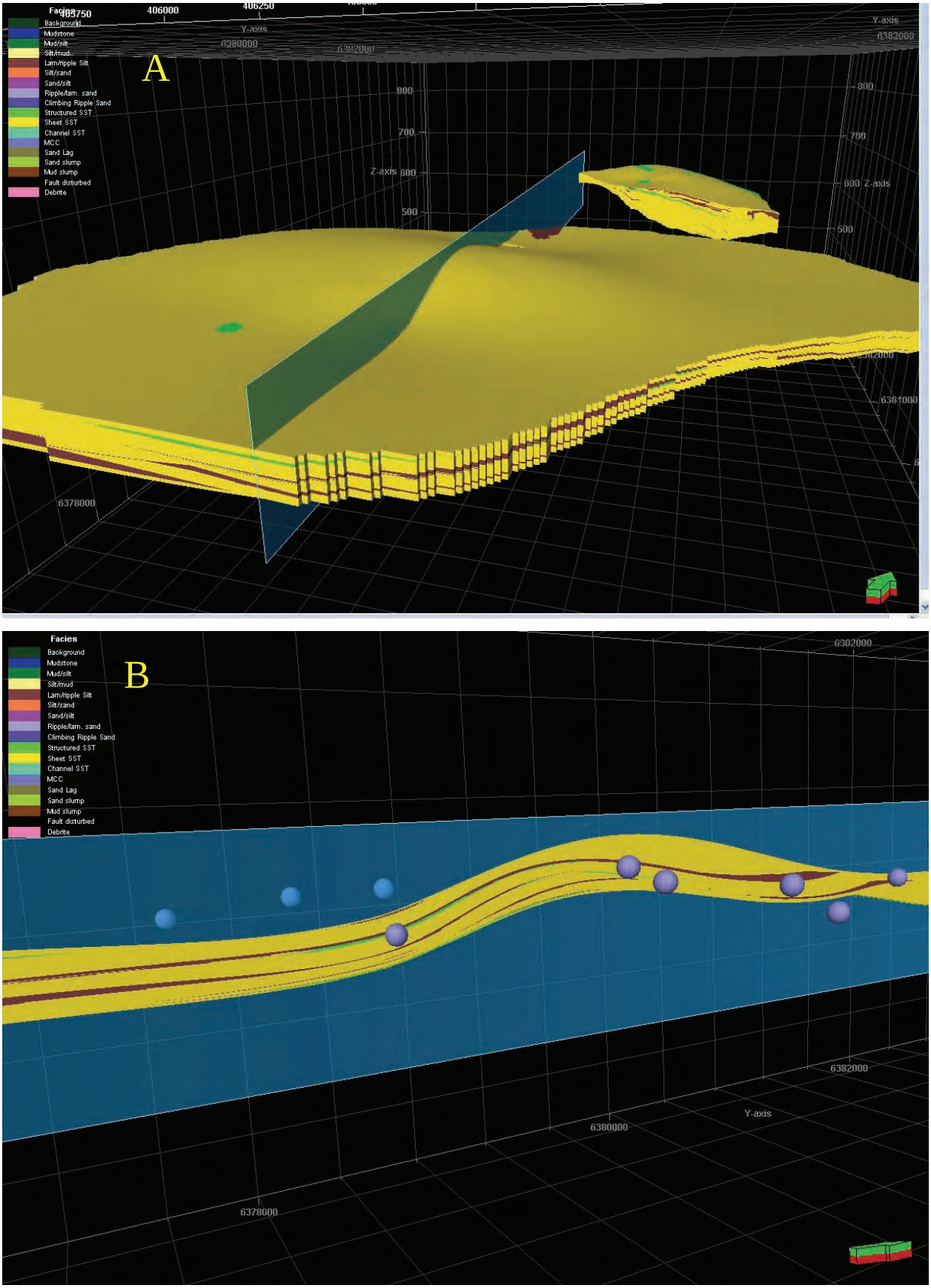

Figure 7.8 The results of the first facies model run, using the Kriging algorithm, and it is immediately evident that too little variation is present (17 lithofaceis were used, yet only 3 are visible). (B) is the cross-section through (A). The purple balls represent well data points.

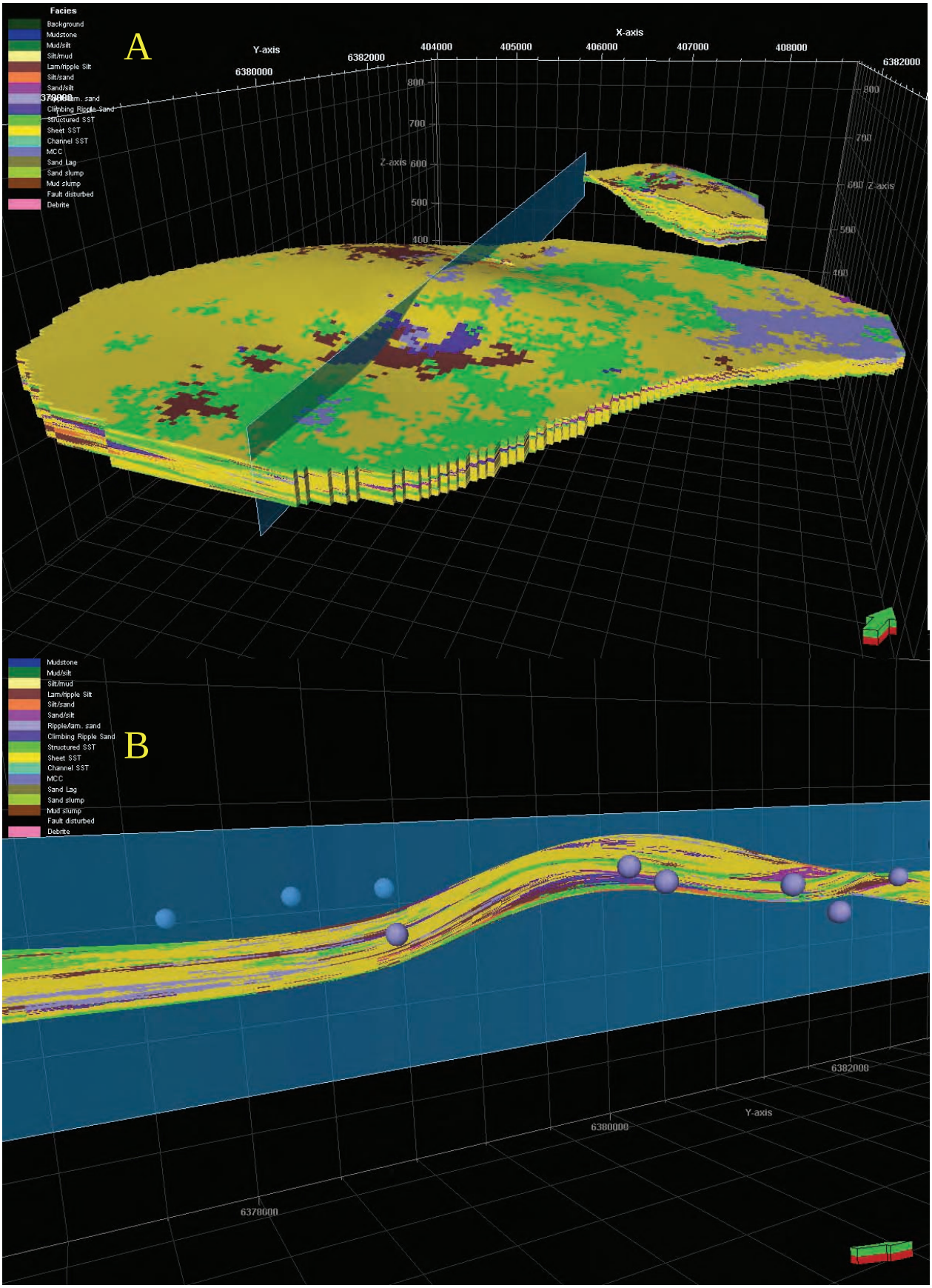

Figure 7.9 The facies model using the Sequential Gaussian algorithm. (B) is the cross-section through (A). Note the large variation in lithofacies that can be observed, as opposed to the Kriging model in Fig 5.12.

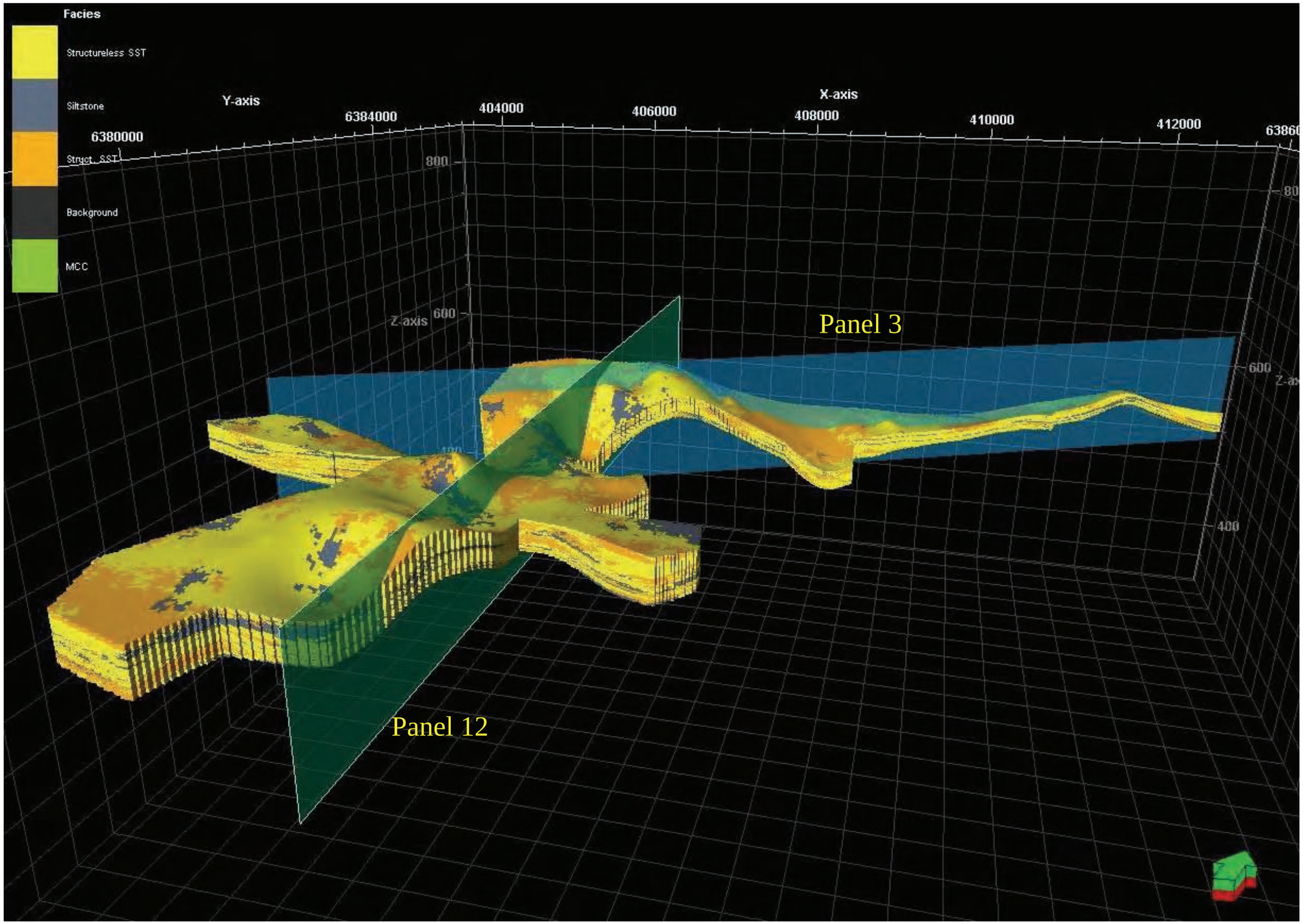

Figure 7.10 The final result. This model was the last to be created. It used the constrained polygon, and the reduced lithofacies. The result was a model that very closely matched the CorelDraw panels. Two cross-sections were created in roughly the same locations as the CorelDraw panels 3 and 12.

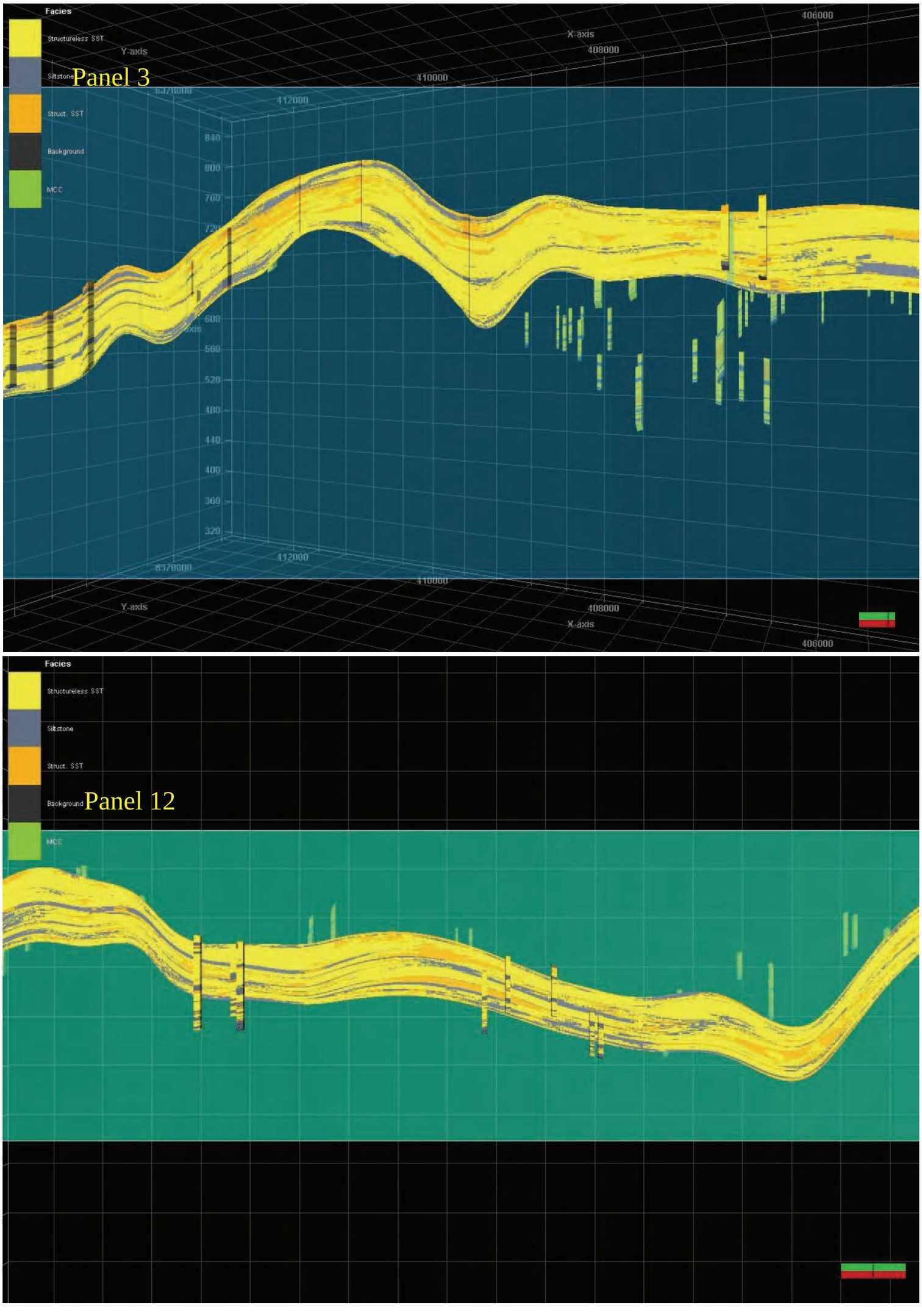

Figure 7.11 Panels 3 and 12 as seen in the final Petrel facies model. Both are at 10 times vertical exaggeration. The blocked (upscaled) wells are shown to relate the accuracy of the overall results to the original data. Overall, the 3D spatial variation remains accurate close to the blocked wells. Panel 12 only roughly matches the CorelDraw panel, as Petrel can only make a cross-section as a straight line.

7.2.6 Limitations encountered during modelling in Petrel

The most obvious limitation of this project's use of Petrel is a processing limitation caused by the computer running Petrel. Some of the algorithms require an immense amount of processing power, as these calculations are done in 3D at relatively high resolutions. For this reason the resolution of 3D objects and models has to be limited, so as to avoid program crashes. An obvious result of this limitation is the loss of thin beds that fall below the resolution of the model. The computer used had a 2.4 Gigahertz (GHz) dual-core processor, 2 Gigabytes (Gb) of RAM, and a 3D gaming graphics card with 256 Mb dedicated memory. As a comparison, the computer used to run Petrel at PetroSA has two 3.2 GHz quad-core CPUs (meaning it is effectively an octa-core CPU), 3 Gb of RAM, and a powerful workstation graphics card with 512 Mb dedicated memory.

When creating surfaces, the algorithms used by Petrel extrapolates the available data based on boundaries provided by the user, either a boundary polygon for an area or the amount of freedom it has around a data point for extrapolation. This can result in some interesting (if completely wrong) trends where data spread is limited. When creating multiple surfaces, these trends can cause overlying surfaces to cross. In this case, the surfaces had to be adjusted in order for processes like the constructing of thickness maps to be successful. The easiest way of confirming accuracy is to ensure that all data points are visible, and are making contact with the surface. This ensures that the minimal amount of data is lost.

Combining the above mentioned limitations, another problem arises. Creating a simple grid based on previous created surfaces, the algorithms will create truncations and pinch-outs where no such features are supposed to exist. This can be overcome by using well-corrections, reducing the well influence radius, and using a more constrained boundary polygon to limit the extrapolation of the algorithms used.

7.3 Results

The main aim of this chapter was to determine whether the field data could be used effectively to produce realistic results, and, if it could, to see how many steps of model building could be

achieved. Unfortunately, it turned out that the data gathered in this project do not lend itself to 3D modelling very well, and modelling could only progress to the creation of a 3D grid. Several factors contribute to this, the most important of which is the distribution. The field area consists mostly of 2D outcrop, with very few deviations from the main trends. While this is especially true for the southern outcrops of the Gemsbok River valley, it does lessen somewhat toward the south into Loskop. While a more 3D distribution can be achieved, a second problem comes in, namely outcrop quality.

The outcrops in the Tanqua Karoo are exceptional, given how well they are preserved and the lack of severe tectonic deformation. However, post-exhumation surface conditions have greatly eroded the available outcrops. This is a problem when trying to correlate outcrop over several kilometres, or even a few hundred metres. Even if correlations are done, the available data might not be complete. The top of Fan 3 is commonly covered or eroded away in several locations, and the base, more often than not, is covered by debris. Also, the interlobe units tend to erode away. These features sometime make it difficult to measure the true vertical extent of individual lobes and lobe-elements.

The red question marks in the Panels (Chapter 3) represent areas where correlations were made, but some degree of uncertainty remains as to the accuracy of these correlations. In many of the thickness maps (Appendix B) a thinning pattern can be seen in the west and south of the sand-prone lobes and lobe-elements. These might not necessarily represent reality. In many cases, they are simply the result of the true thickness of a unit being unknown. The correction of this problem introduces some degree of uncertainty for in-depth data analyses.

The Petrel work did turn out fairly well, under the circumstances. Figure 7.12 illustrates the relative accuracy achieved with the final facies model, at least in respect of the up-scaled wells. The up-scaled wells were also fairly true to the original data (Fig. 7.7). Figures D.3, D.4 and D.5 in Appendix C are the Petrel equivalents of Panels 1 – 2, 3 and 12. All of these show the original lithofacies as well as the new lithofacies. They were also created using the new Excel data. The extended data are most visible at the base. Some error still slipped in, but thanks to the Z-adjustments made, these did not affect the final product significantly, if at all.

In all, the Petrel work served to prove several points:

1. The quality and nature of the input data are critical. While good data can be gained from a 2D outcrop, or even 1D well-logs, without decent 3D spread of data it is near impossible to get a truly accurate and reliable representation of information in 3D data analysis.
2. Close quality control of the data and results is important. Modelling is a highly iterative process, and errors can occur at any level of the process.
3. The scale at which 3D data analyses can be done relies heavily on the hardware that is available. Without decent computing ability much data can be lost simply because of too low resolutions. This can have major consequences when the presence or absence of barriers to hydrocarbon movement is critical to the productivity of a field.
4. Knowing what to use and where to use it makes the final output more reliable.

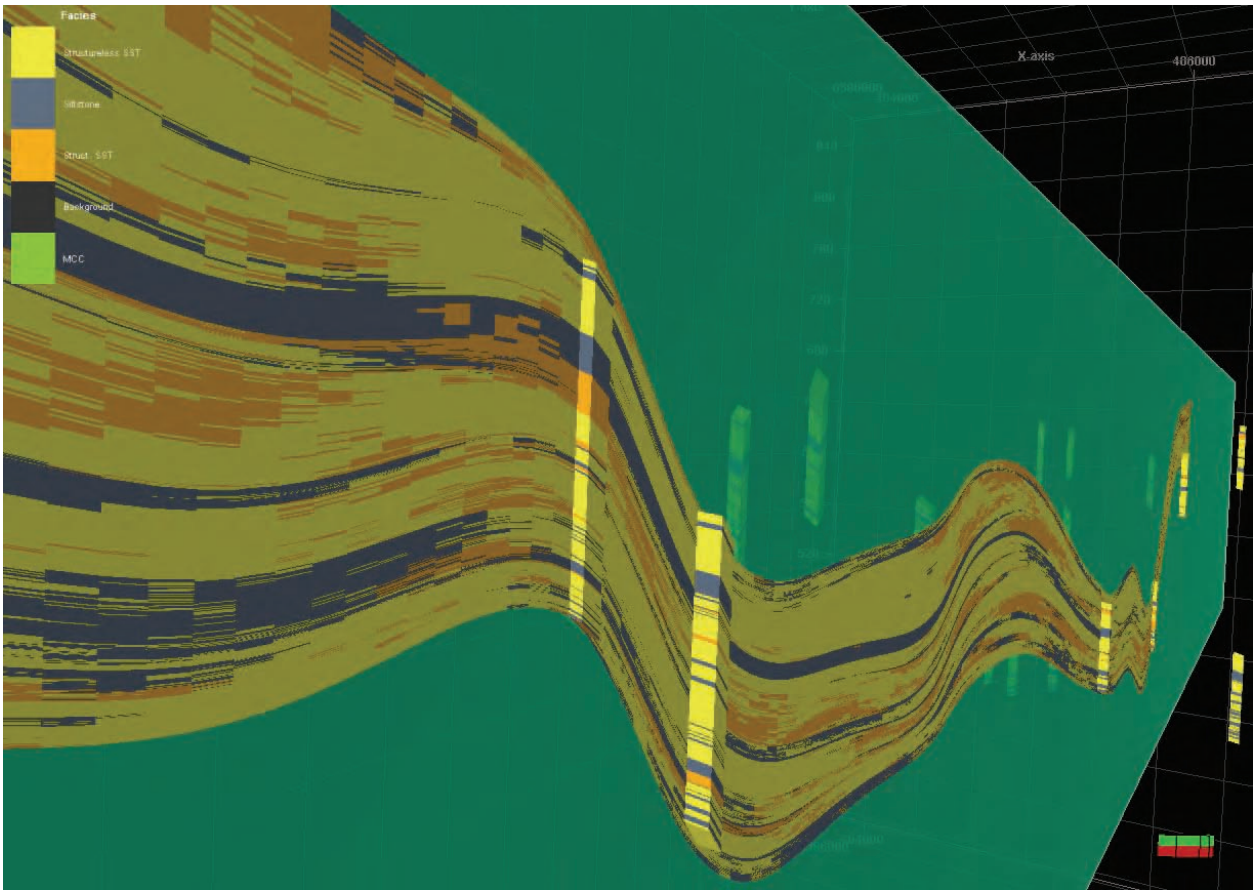

Figure 7.12 This figure attempts to show the accuracy with which Petrel created the facies model in regards to the up-scaled wells. With enough wells to constrain the algorithms, Petrel can produce accurate and realistic facies models

Chapter 8

Conclusions

Conclusions

8.1 High resolution outcrop maps and data incorporation

Two secondary aims of this study were to produce high resolution outcrop maps, detailing the internal architecture, lithofacies associations and characteristics of mid-fan Fan 3, and the incorporation of data collected during the Lobe project. The two main aims of this study, however, depended on the information gained from these two aims, as these aims represent the first analyses and interpretations of the data.

The 2D outcrop correlation panels (Chapter 3) focussed mainly on the stratigraphy and lithofacies distribution of the study area, giving a visual representation of the lobes and lobe-elements identified in Fan 3. These panels formed the basis for all subsequent work with the data.

The information from the Lobe project provided much to this study, including: definitions and nomenclature for features identified within Fan 3; the basic stratigraphy of Fan 3 as applied to the northern outcrops; and the architecture and depositional behaviour of Fan 3 to the north of the Gemsbok River valley. The results of the Lobe project are presented in Prélat *et al*. (in review) and in the Final Lobe Report (web-based reference 1). The results, as well as some of the results of this study, have also been presented at the AAPG 2008 International Conference and Exhibition in Cape Town, South Africa, between 26 and 29 October. The posters are presented in Appendix A, with this study represented in section C.1. A pre-completion presentation of this project was given to PetroSA, as part of the agreement for their assistance with Petrel. The PowerPoint slides are presented in Appendix B.

The Lobe project identified 6 lobes which constitute mid to distal Fan 3 to the north of the Gemsbok River valley. Only five of these lobes were identified to the south (Lobe 3 is not present), as well as an additional lobe and a grouping of low volume turbidites at the base of the succession. They mark the start of the progradational stage of the fan's deposition. The aggradational stage is represented by Lobe 2 through Lower Lobe 5. The retrogradational stage saw the deposition of Upper Lobe 5 and Lobe 6.

8.2 Channelised lobe to sheet deposit transition

The main aim of this study was to assess the transition of channelised lobe deposits into sheet deposits. This aim is dependent on the field results of the project, namely the high-resolution vertical profiles, outcrop correlation panels and computer generated isopach maps, as well as the information from current and previous studies.

While a single lobe could not be systematically analysed from the proximal to distal end, due to factors such as outcrop discontinuity, the Gemsbok River valley provides a unique opportunity. The comprising lobes of Fan 3 are all exposed, and each lobe represents a strike section through a different part of an idealised lobe (Fig. 6.6). Working from the top down, Lobe 6 represents the channelised zone. Progressing further into the fan section, Lower Lobe 5, Lobe 4 and Lobe 2 gradually become more distributive and distal. Lobe 1 represents the near-pinch-out scenario. The basic pattern for fan deposition is channels in the proximal sections, going into channelised sheets as the flow looses strength and exits confinement. As the channelised sections leave confinement, they become distributive in the frontal splay section. The exact direction of distribution for each flow is determined by several factors (topography being the main determining factor). Where a lobe has a finger-shaped depositional pattern, sheet deposits are only present along the margins, or in-between the axial zones that are far enough apart. The fringe areas of a lobe with finger-shaped depositional patterns tend to have relatively extensive deposits of linked-debrites, representing the final sediments deposited.

8.3 Conceptual depositional model

Using palaeocurrent patterns, as well as the architectural elements of Fan 3, some of the autogenic control for the deposition of Fan 3 appeared to be topographical barriers to local flow and deposition of lobes. Most of the lobes displayed a curved depositional path. It was suggested that the initial path was due to the presence of Fan 2 near the feeder area of Fan 3.

While compensation between the lobes can explain the off-set positions of Upper Lobe 5 and Lobe 6, the shift in palaeoflow suggests something else affecting the deposition of the lobes of Fan 3. The subsequent shift in palaeoflow from north-east to north-west was attributed to some unidentified topographical feature in the west and south that restricted the linear flow of the

lobes. Lobe 6 saw an inferred slight north-westward shift in feeder area, as well as a more eastern palaeoflow direction. Eventually it also turned north, but the presence of its only identified axial zone so far off-set from the other lobes suggested that the eastern barrier was at least partly overcome.

No channels, as described by Johnson *et al*. (2001), were identified in the study area. Several channelised sheets (Highly amalgamated zones of Hodgson *et al*., 2006) were identified. The Gemsbok River valley could be used as an analogue for the channelised sheet to sheet deposit transition. The lobes that are exposed here show features ranging from distal to the transition from channelised to sheet deposits, thanks to the nature of their deposition.

Some allogenic control, such as relative sea-level fluctuation, could be inferred from the pro- to retrogradation pattern of deposition for Fan 3. Each lobe corresponds to an early LST, followed by a brief flooding period dominated by fine-grained deposition. A LST represents a reduction in accommodation space, and subsequently a reduction in the sediment load that currents can carry. The result is the deposition of thick sand-prone units. Evidence for allogenic control comes from observation by Prélat *et al*. (in review), stating that the interlobe siltstones do not laterally grade into sandstone, which they interpret as a decrease in sediment supply.

From the above results it is evident that a combination of allogenic and autogenic controls influenced the deposition of Fan 3. Also, each lobe (or even lobe-element) shows a distinctly different depositional pattern. A single depositional model can therefore not sufficiently describe the whole of Fan 3. However, some simplification is possible. The progradational phase saw the deposition of “classic” lobe architectures, confined to what appears to be a topographical low. The aggradational phase, and even the retrogradational phase, saw the deposition of lobes take on the finger-shape as described by Machado *et al*. (2004).

8.4 Computer modelling with Petrel

The computer work with Petrel produced some useful isopach maps (Appendix C). However, it was determined that the linear nature of the outcrops in the study area presented a problem for the construction of a static 3D model. The quality and nature of the data used for the creation of 3D models are critical. Good data can be gained from 2D outcrop, or even 1D well-logs, but

without a decent 3D spread of data it is near impossible to get a truly accurate and reliable representation of information in 3D data analysis. This is because the algorithms used by programs like Petrel have to extrapolate data away from fixed data points. If not enough data are present to constrain the extrapolation, the algorithms cannot realistically predict what a trend should be.

It was found during the iterative process of modelling that computing power also plays an important role. The ability to create highly detailed renderings requires large amounts of computing power. Without decent computing ability much data can be lost simply because of too low resolutions. In terms of real-world situations, this can have major consequences in industry when the presence or absence of barriers to hydrocarbon movement is critical to the productivity of a field.

Even though the data proved to be unsuitable, it is not unusable. If more three-dimensional constraint can be provided by behind-outcrop methods, such as core-wells and ground-penetrating radar, the data could probably be used to greater effect.

References

Alexander, J., Morris, S. (1994) Observations on experimental, non-channalized, high-concentration turbidity currents and variation in deposits around obstacles. *Journal of Sedimentary Research*, 64: 899 - 908

Basu, D., Bouma, A.H. (2000) Thin-Bedded Turbidites of the Tanqua Karoo: Physical and Depositional Characteristics. *A. H. Bouma and C. G. Stone, eds., Fine-grained turbidite systems*. AAPG Memoir 72/SEPM Special Publication, 68: 263 - 278.

Boggs, S. Jr (2001) Principles of Sedimentology and Stratigraphy. Prentice Hall, 726 pp. 3rd Edition

Bouma, A.H. (1962) Sedimentology of some Flysch Deposits: A Graphic Approach to Facies Interpretation. Elsevier, Amsterdam, 168 pp

Bouma, A.H., Wickens, H. de V. (1991) Permian passive margin submarine fan complex, Karoo Basin, South Africa: possible model to Gulf of Mexico. *Gulf Coast Association Geological Societies Transactions*, 41: 30 – 42

Deptuck, M.E., Piper, D.J.W., Savoye, B., Gervais, A. (2008) Dimensions and architecture of late Pleistocene submarine lobes off the northern margin of East Corsica. *Sedimentology*: 1 - 32

Deutsch, C.V., Xie, Y., Cullick, A.S. (2001) Surface geometry and trend modelling for integration of stratigraphic data in reservoir models. 2001 Society of Petroleum Engineers Western Regional Meeting, March 20 – 30, Bakersfield, California, SPE Paper 68817

Fildani, A., Drinkwater, N.J., Weislogel, A., McHargue, T., Hodgson, D.M., Flint, S.S. (2007) Age controls on the Tanqua and Laingsburg deep-water systems: new insights on the evolution and sedimentary fill of the Karoo basin, South Africa. *Journal of Sedimentary Research*, 77: 901 – 908

Gardner, M.H., Sonnenfeld, M.D. (1996) Sequence stratigraphy and eolian-derived turbidites: Patterns of deep-water sedimentation along an arid carbonate platform, Permian (Guadalupian) Delaware Mountain Group, West Texas. *Permian Basin exploration and production*

strategies: Applications of sequence statigraphy and reservoir characterization concepts. West Texas Geological Society Bulletin, 92-91: 7 - 12

Gardner, M.H., Borer, J.M., Melick, J.J., Mavilla, N., Dechesne, M., & Wagerle, R.N. (2003) Stratigraphic process-response model for submarine channels and related features from studies of the Permian Brushy Canyon outcrops, West Texas. *Marine and Petroleum Geology*, 20, 757 - 787

Haldorsen, H.H., Lake, L.W. (1984) A new approach to shale management in field-scale model. *Society of Petroleum Engineers Journal*, April: 447 - 457

Haldorsen, H.H., Chang, D.W. (1986) Notes on stochastic shales; from outcrop to simulation model. *In* L.W. Lake and H.B. Caroll, eds., Reservoir characterization: London, Academic Press: 445 – 485

Haughton, P.D.W., Barker, S.P., McCaffrey, W.D. (2003) 'Linked' debrites in sand-rich turbidite systems – origin and significance. *Sedimentology*, 50: 459 – 482

Hodgson, D.M., Flint, S.S., Hodgetts, D., Drinkwater, N.J., Johannessen, E.J., Luthi, S.M. (2006) Stratigraphic Evolution of Fine-Grained Submarine Fan Systems, Tanqua Depocenter, Karoo Basin South Africa. *Journal of Sedimentary Research*, 76: 19 - 39

Johnson, A.M. (1970) Physical Processes in Geology. Freeman, Cooper, San Francisco, CA, 577 pp.

Johnson, M.R., van Vuuren, C.J., Hegenberger, W.F., Key, R., Shoko, U. (1996) Stratigraphy of the Karoo Supergroup in southern Africa: an overview. *Journal of African Earth Sciences*, 23: 3 - 15

Johnson, S.D., Flint, S., Hinds, D., Wickens, H. de V. (2001) Anatomy, geometry and sequence stratigraphy of basin floor to slope turbidite systems, Tanqua Karoo, South Africa. *Sedimentology*, 48: 987 - 1023

Johnson, S.D., Hadler-Jacobsen, F. (2001) Field Guide for AAPG Hedberg Field Research Conference: Deep –Water Sandstones, Tanqua Karoo, South Africa. Den Norske Stats Olje Selskap: STATOIL

King, R., Van Lente, B., Potts, G., Hodgson, D.M., Andersson, P.O.D., Worden, R.H., Flint, S.S., Wickens, H. de V. (2004). Extra-foreland source to turbidite sink in the early Karoo Basin, South Africa. *AAPG Annual Meeting 2004: Embrace the Future, Celebrate the Past Technical Program*

Kneller, B., Buckee, C. (2000) The structure and fluid mechanics if turbidity currents: a review of some recent studies and their geological implications. *Sedimentology*, 47: 62 - 94

Lane-Serff, G.F., Beal, L.M., Hadfield, T.D. (1995) Gravity current flow over obstacles. *Journal of Fluid Mechanics*, 292: 9 - 53

Lowe, D.R. (1982) Sediment gravity flow: II. Depositional models with special reference to the deposits of high-density turbidity currents. *Journal of Sedimentary Research*, 52: 279 – 297

Luthi, S.M., Hodgson, D.M., Geel, C.R., Flint, S. S., Goedbloed, J.W., Drinkwater, N.J., Johannessen, E.P. (2006) Contribution of research borehole data to modelling fine-grained turbidite reservoir analogues, Permian Tanqua–Karoo basin-floor fans (South Africa). *Petroleum Geoscience*, 12: 1 - 16

Machado, L.C.R., Kowsman, R.O., de Almeida Jr., W., Murakami, C.Y., Schreiner, S., Miller, D.J., Orlando, P., Piauilino, V. (2004) Geometry of the proximal part of the modern turbidite depositional system of the Carapebus Formation, Campos Basin: a model for reservoir heterogeneities. *B. Geoci. Petrobras, Rio de Janeiro*, 12, no. 2: 287 - 315

Miall, A.D., 1995. Description and interpretation of fluvial deposits: a critical perspective. *Sedimentology*, 42: 379 - 384

Middleton, G. V., Hampton, M. A. (1973) Part I. Sediment gravity flows: mechanics of flow and deposition. In *Turbidites and Deep Water Sedimentation*, ed. G. V. Middleton, A. H. Bouma, *SEPM Pac. See. Short Course Notes.* Anaheim, Calif: SEPM. 38pp.

Middleton, G. V., Hampton, M. A. (1976) Subaqueous sediment transport and deposition by sediment gravity flows. In *Marine Sediment Transport and Environmental Management*, ed. D. J. Stanley, D. J. P. Swift, pp. 197 - 218. New York: Wiley

Mutti, E. (1992) Turbidite Sandstones. *Agip and Instituto di Geologia*, Univ. Parma, 275

Nardin, T.R., Gorsline, D.S., Edwards, B.D. (1979) Santa Cruz Basin, California borderland: Dominance of slope processes in basin sedimentation. *Geology of continental slopes: Soc. Econ. Paleontologists and Mineralogists Specieal Publications*, 27: 208 – 221

Paulissen, W. (2007) The geometry of lobe elements in Basin-Floor Fan 4, Tanqua Karoo Basin, South Africa: M.Sc. Thesis, Delft University of Technology, The Netherlands, 98 pp

Pickering, K.T., Hiscott, R.N., Hein F.J. (1989) Deep Marine Environments: Clastic Sedimentation and Tectonics. London. Unwin Hyman.

Posamentier, H.W., Jervey, M.T., Vail, P.R. (1988) Eustatic controls on clastic deposition I – Conceptual framework. *Sea-level changes: an integral approach*. SEPM Special Publications, 42: 109 - 124

Posamentier, H.W., Vail, P.R. (1988) Eustatic controls on clastic deposition II – Sequence and system tracts models. *Sea-level changes: an integral approach*. SEPM Special Publications, 42: 125 – 154

Prather, B.E., Booth, J.E., Steffens, G.S., Craig, P.A. (1999) Classification, calibration and stratigraphic succession of seismic facies from intraslope basins, deep water Gulf of Mexico. *AAPG Bulletin*, 83: 721 - 727

Prélat, A (2006) Sedimentology and stratigraphy of Unit B around the Heuningberg anticline, Permian Laingsburg Formation, Southwestern Karoo Basin, South Africa. M.Sc. Thesis, University of Stellenbosch, South Africa, 160 pp.

Prélat, A., Hodgson, D.M., Flint, S.S. (2008) Evolution, architecture and hierarchy of distributary deep-water deposits: a high-resolution outcrop investigation of submarine lobe deposits from the Permian Karoo Basin, South Africa. *In review*

Pyrcz, M.J., Deutsch, C.V. (2003) Stochastic surface modelling in mud-rich, fine-grained turbidite lobes (abs.): AAPG Annual Meeting, May 11 – 14, Salt Lake City, Utah, Extended abstract, http://searchanddiscovery.net/documents/abstracts/annual2003/extend/77965.PDF, 6p

Pyrcz, M.J., Catuneanu, O., Deutsch, C.V. (2005) Stochastic surface based modelling of turbidite lobes. *AAPG Bulletin*, 89, 2: 177 - 191

Remacha, E., Fernandez, L.P. (2003) High-resolution correlation patterns in the turbidite systems of the Hecho Group (South-Central Pyrenees, Spain). *Marine and Petroleum Geology*, 20, 711 - 726

Rubidge, B.S., Modesto, S., Sidor, C., Welman, J. (1999) Eunotosaurus africanus from the Ecca–Beaufort contact in Northern Cape Province, South Africa - implications for Karoo Basin development. *South African Journal of Science*, 95: 553 – 555

Scott, E.D. (1997) Tectonics and sedimentation: evolution, tectonic influences and correlation of the Tanqua and Laingburg sub-basins, southwest Karoo Basin. Ph.D thesis, Louisiana State Uinversity. 234 pp

Shanmugam, G. (1980) Rhythms in deep sea, fine-grained turbidite and debris-flow sequences, Middle Ordovician, eastern Tennessee. *Sedimentology*, 27: 419 - 432

Shanmugam, G. (1997a) The Bouma sequence and the turbidite mind set. *Earth-Science Reviews*, 42: 201 - 229

Shanmugam, G. (2000) 49 years of the turbidite paradigm (1950s – 1990s): deep-water processes and facies models - a critical perspective. *Marine and Petroleum Geology* 17: 174 - 231

Sixsmith, P.J. (2000) Stratigraphic development of a Permian turbidite system on a deforming basin floor: Laingsburg Formation, Karoo Basin, South Africa. Ph.D Thesis, University of Liverpool, 229 pp.

Stouthamer, E., Berendsen, H. J. A. (2007) Avulsion: the relative roles of autogenic and allogenic processes. *Sedimentary Geology*, 198: 309 - 325

Stow, D.A.V., Johansson, M. (2000) Deep-water massive sands: nature, origin and hydrocarbon implications. *Marine and Petroleum Geology*, 17: 145-174

Stow, D.A.V., Mayall, M. (2000) Deep-water sedimentary systems: New models for the 21st century. *Marine and Petroleum Geology*, 17: 125 – 135

Stow, D.A.V., Shanmugam, G. (1980) Sequences of structures in fine-grained turbidites: comparison of recent deep-sea and ancient flysch sediments. *Sedimentary Geology*, 25: 23 - 42

Sullivan, M., Formeman, J. L., Jennette, D., Stern, D., Gerrick, N. J., Goulding, F. J. (2004) An integrated approach to characterization and modeling deep-water reservoirs, Diana Field, Western Gulf of Mexico, an integration of outcrop and modern analogs in reservoirs modeling. *AAPG Memoir*. 80, 215-234

Talling, P.J., Amy, L.A., Wynn, R.B., Peakall, J., Robinson, M. (2004) Beds comprising debrite sandwiched within co-genetic turbidite: origin and widespread occurrence in distal depositional environments. *Sedimentology*, 51: 163 – 194

Van Lente, B. (2004) Chemostratigraphic trends and provenance of the Permian Tanqua and Laingsburg depocentres, South Western Karoo Basin, South Africa: Ph.D. Thesis, University of Stellenbosch, South Africa, 339 pp

Van Wagoner, J.C., Posamentier, H.W., Mitchum, R.M. Wail, P.R., Sarg, J.F., Louitit, T.S., Hardenbol, J. (1988) And overview of the fundamentals of sequence stratigraphy and key definitions. *Sea-level changes: an integral approach*. SEPM Special Publications, 42: 40 - 45

Van Wagoner, J.C. (1995) Sequence stratigraphy and marine to non-marine facies architecture of foreland basin strata. *Sequence stratigraphy of foreland basin deposits: outcrop and subsurface examples from the Cretaceous of North America*. AAPG Memoir 64: 137 - 223

Turner, B.R. (1999). Tectonostratigraphical development of the Upper Karoo foreland basin: orogenic unloading versus thermally-induced Gondwana rifting. *Journal of African Earth Sciences*, 28, 215–238

Van der Merwe, W.C. (2004) Facies architecture and variation of the Hangklip Fan in the Bizansgat and Klein Hangklip area, Tanqua Sub-basin, South Africa. Honours Thesis, University of Stellenbosch, South Africa, 118 pp.

Van der Merwe, W.C. (2006) Stratigraphy and facies architecture of the uppermost fan system in the Tanqua sub-basin, Permian Ecca Group, South Africa. M.Sc. Thesis, University of Stellenbosch, South Africa, 197 pp.

Van der Werff, W., Johnson, S. (2003) High resolution stratigraphic analysis of a turbidite system, Tanqua Karoo Basin, South Africa. *Marine and Petroleum Geology*, 20:45-69

Viljoen, J.H.A., Wickens, H. de V. (1992) Lithostratigraphy of the Vischkuil Formation (Ecca Group). *Geological Survey of South Africa, Lithostratigraphic Series*, 19, 7 pp

Visser, J.N.J. (1993) Sea-level changes in a back-arc forearc transition – The Late Carboniferous-Permian Karoo Basin of South Africa. *Sedimentary Geology*, 83: 115 – 131

Wickens, H. de V. (1984) Die stratigrafie en sedimentologie van die Groep Ecca wes van Sutherland: M.Sc. Thesis, University of Port Elizabeth, South Africa, 86 pp

Wickens, H. De V., Brink, G.J., van Rooyen, W. (1990) The sedimentology of the Skoorsteenberg Formation and its applicability as a model for submarine fan turbidite deposits in the Bredarsdorp Basin. Rep. Soekor, Parow, 47pp

Wickens, H. de V., Bouma, A.H. (1991a). A passive margin-type submarine fan complex, Permian Ecca Group, South Africa. *American Association of Petroleum Geologists Bulletin*, 75, p. 693

Wickens, H. de V. & Bouma, A.H. (1991b). The Tanqua submarine fan complex, Permian Ecca Group, South Africa. *American Association of Petroleum Geologists Bulletin*, 75, p. 522.

Wickens, H. de V. (1994) Basin Floor Fan building Turbidites of the South-western Karoo Basin, Permian Ecca Group, South Africa. Ph.D. thesis, University of Port Elizabeth. pp. 233

Wickens, H. de V., Bouma, A.H. (2000) The Tanqua Fan Complex, Karoo Basin, South Africa - Outcrop Analog for Fine-Grained, Deepwater Deposits. *A. H. Bouma and C. G. Stone, eds., Fine-grained turbidite systems, AAPG Memoir 72/SEPM Special Publication*, 68: 153–164

Wild, R., King, R., Van Lente, B., Flint, S., Hodgson, D., Potts, G., Wickens, H. de V. (2004). *Slope project first year report and field guide*. The Stratigraphy Group, Department of Earth and Ocean Sciences, University of Liverpool, United Kingdom & Department of Geology, University of Stellenbosch, South Africa. Part A, pp. 65

Wild, R.J., Hodgson, D.M., Flint, S.S., 2005. Architecture and stratigraphic evolution of multiple, vertically-stacked slope channel complexes, Tanqua depocenter, Karoo Basin, South Africa. In: Submarine Slope Systems, Processes and Products, Hodgson & Flint (eds.). *Geological Society, London, Special Publications*, 244: 89 – 112

Wynn, R.B., Weaver, P.P.E., Masson, D.G., Stow, D.A.V. (2002) Turbidite depositional architecture across three interconnected deep-water basins on the north-west African margin. *Sedimentology*, 49: 669 - 695

Web based references

1. Hodgson, D.M., Prélat, A., Groenenberg, R., Paulissen, W., Flint, S.S. (2008) Final Lobe Report: http://pcwww.liv.ac.uk/strat/lobe

Appendix A

AAPG Poster

AAPG Poster

The poster presented here was presented by Liverpool University at the AAPG International Conference and Exhibition, held in Cape Town from 26 to 29 October 2008. As part of the Lobe project, some of the work done in this project was presented in Section C1 of the poster. Other presenters for the poster were Dave Hodgson, Amandine Prélat, and Rochelle Steyn. The work of Remco Groenenburg, Wieske Paulissen from Delft University, as well as Stefan Luthi, was also presented.

Geological reservoir modelling and process-based numerical modelling of deep-water distributive systems from detailed outcrop data:

examples from the Tanqua depocentre, South Africa

Hodgson, D.M.[1], Prelat, A[1]., Groenenberg, R.[2], Paulissen, W.E.2, Luthi, S.M.[2], Neethling, J.[3], Steyn, R.[3], Wickens, DeV.[3]

[1] Stratigraphy Group, Department of Earth and Ocean Sciences, 4 Brownlow Street, University of Liverpool, Liverpool, UK
[2] Department of Geotechnology, Delft University of Technology, The Netherlands
[3] Department of Geology, Geography, and Environmental Studies, Cnr Ryneveld and Merriman Streets, Stellenbosch, Western Cape, South Africa

A. Introducing the problem and the tools used

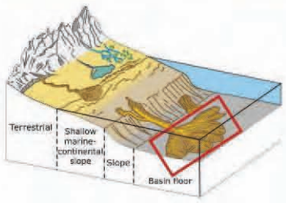

Terminal submarine fan lobes are distributive systems at the most down-dip depositional position of terrigenous sediment transported by gravity flows through basin margins. As such, they form an important, if cryptic, record of the interplay between climatic, eustatic and tectonic controls on the transfer of sediment from land to ocean. Distributive systems are dominated by depositional processes, although erosional processes are still important.

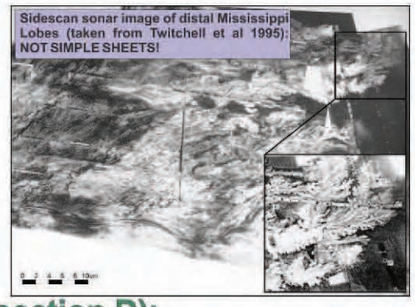

A1. Key questions:

On the shape, dimensions and geometries of lobe deposits (section B):

- What is the architectural hierarchy of elements in distributive systems?
- What is the depositional shape, dimensions and stacking patterns of lobe deposits?

On the prediction of the subsurface (section C):

- Can small-scale outcrop data be effectively imported and represented in 3D modeling software?
- Does the resulting output data remain true to the input data after upscaling of facies?

On the control on geometry and stacking patterns of the lobe deposits (section D):

- What controls the stacking of lobes and lobe elements?
- Are the stacking patterns and hierarchy identified at outcrop possible to simulate using a forward modelling approach?
- What is the interplay of autogenic and allogenic controls required to produce the lobe geometries, stacking patterns and volumes observed in the Karoo deposits?

A2. Tools for answering:

B. Geological model

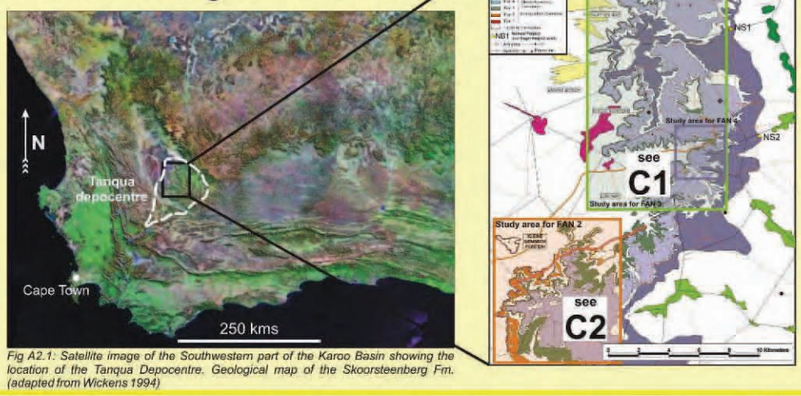

Fig A2.1: Satellite image of the Southwestern part of the Karoo Basin showing the location of the Tanqua Depocentre. Geological map of the Skoorsteenberg Fm. (adapted from Wickens 1994)

Outcrops of the Permian Tanqua depocentre were chosen because of their strike and dip continuity and good accessibility. They allow detailed study from bed to system scale.

The **Tanqua depocentre** is situated in the southwestern corner of the Karoo Basin and records sedimentation ins a retroarc forewland basin during the late Paleozoic and early Mesozoic. The Skoorsteenberg Formation (**~255 Ma; Fildani et al. 2007**), the focus of this study, consists of four basin floor fans and one lower slope to base of slope unit.

- **Fan 2** was studied to document the changes in stratigraphy and sedimentology towards a fan pinch-out within a distal fan setting *(MSc work of Rochelle Steyn in* **POSTER C2)**
- **Fan 3** was studied in its most distal areas (starting 15 km from frontal pinchout). The aim is to document the evolution, architecture and hierarchy of lobe deposits *(MSc work of Jaco Neethling in* ***POSTER C1****/ PhD work of Amandine Prélat in* ***POSTER B****.)*
- Two static reservoir models were built for **Fan 4** from 49 sedimentary logs and the NB2 boreholes *(MSc work of Wieske Paulissen in* ***Poster E****).*

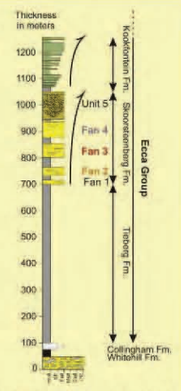

Fig A2.2: Schematic stratigraphic column of the Tanqua depocentre.

C: Reservoir modelling: *Petrel*

Petrel is used to build a 3D view of the studied geobodies. Fans 2, 3 and 4 were investigated and static reservoir models were built for each from sedimentary logs collected in the field:

- The data from 91 sedimentary logs were collected over the Fan 2 study area of 12 x 5 km. The data was used to generate a facies model for sandstone lobe- and siltstone inter-lobe elements for Middle Fan 2.
- The data from 72 sedimentary logs collected in the Fan 3 study area of 8 x 6 km was used to generate a facies model of 6 sandstone lobes .
- The data from 49 sedimentary logs in Fan 4 was also investigated.

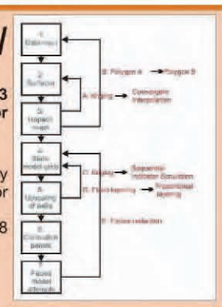

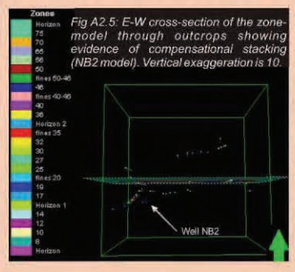

Fig A2.5: E-W cross-section of the zone-model through outcrops showing evidence of compensational stacking (NB2 model). Vertical exaggeration is 10.

Isopach thickness maps:

Isopach maps are generated by subtracting surfaces from each other. Often, geobodies have a larger extent than the isopachs map boundaries. Generally, trends can be drawn when coupled with palaeocurrents.

Simple grids:

Grids were created to define a 3D frame of reference for the study areas using surfaces. The grid allows each of the lobes or lobe elements defined at outcrop to be described as a zone in Petrel. Each zone is further subdivided into layers to simulate internal variation. The zone models represent several levels in the hierarchy of the lobe complex, and may provide insights into the trends of the zones and their stacking patterns.

Facies Modelling:

Based on the upscaled well-logs containing facies and facies associations, facies distributions can be visualized in 3D. Correlation panels, a 2D representation, can illustrate the differences between input and output data.

D: Process-based modelling: *FanBuilder*

The aim is to test some of the concepual models derived from outcrop observations, and to try and constrain some of the input parameters that governed the flow of the turbidity currents and the depositional architecture observed in the ancient distributive system.

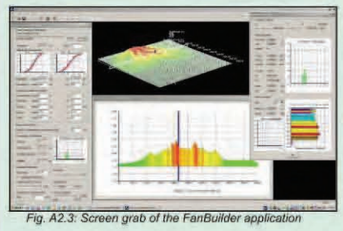

Fig. A2.3: Screen grab of the FanBuilder application

FanBuilder is a generic 3D process-based model capable of simulating the construction of fan stratigraphy by sequential turbidity-current events.

The core of the FanBuilder application patterns a process-based model capable of simulating turbidity-current flow behaviour and resulting sedimentation.

Input parameters are: initial topography, tectonic activity, grain size distribution, concentrations, magnitude and frequency of the flows.

The validation step is an essential step in the development of any model. During validation, the quality of the model is assessed and, preferably, quantified by comparing simulated results to a truth-case. Here, the truth-case is a laboratory experiment (Luthi, 1981), in which a mixture of water and suspended sediment flows out from a supply channel onto an expansion table (see Figure 4A) in the form of a small-scale turbidity current. The experiment itself may be considered to represent a downscaled version of turbidity currents that occur in nature, with a scaling of 1:103 to 1:105.

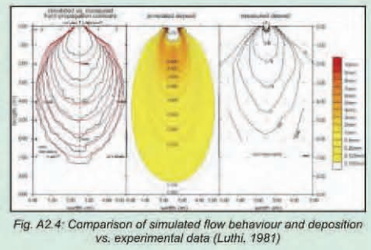

Fig. A2.4: Comparison of simulated flow behaviour and deposition vs. experimental data (Luthi, 1981)

B. INTERNAL ARCHITECTURE AND ORGANISATION OF TERMINAL LOBE DEPOSITS

B1. Hierarchy

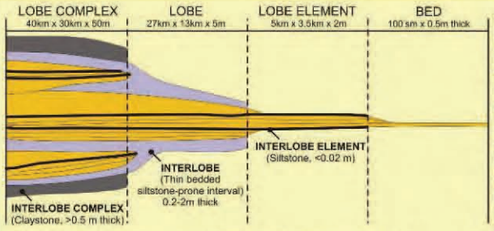

Fig. B1.1:Hierarchical element scheme for distributive systems based on Fan 3.

The development of a hierarchy of architectural elements that stack to construct a distributive deep-water system begins with identification of different types of bounding surfaces and/or fine-grained units.

- The fundamental building block in the stratigraphy of a distributive system is the ***bed***, which represents a single depositional event.
- One or more beds or bedsets stack to form a sand-rich ***lobe element***, which is separated from another lobe element by a locally eroded <0.02 m thick siltstone.
- One or more genetically related lobe elements stack to form a ***lobe***, which are typically 4-10 m thick, and several kilometres long and wide, and elongate in a downstream direction.
- Lobes are separated by fine-grained thin-bedded intervals that maintain similar facies and thickness for >8km in dip and strike sections, and are referred to as ***interlobes***.
- One or more genetically-related lobes stack to form a ***lobe complex*** (eg Fan 3). Lobe complexes are typically 30-60 m thick and bounded by 2-20 m thick claystones.

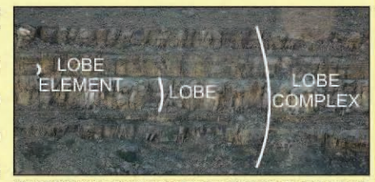

Fig. B1.2: Outcrop photograph of the Fan 3 showing the hierarchy of lobe element, lobe and lobe complex.

B2. Facies Distribution

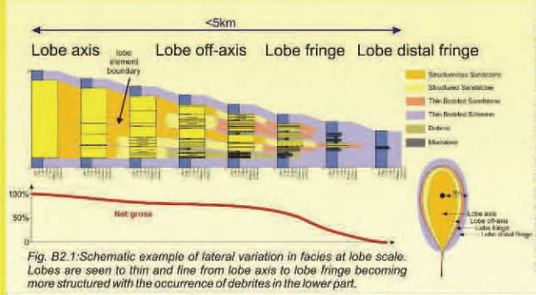

Fig. B2.1:Schematic example of lateral variation in facies at lobe scale. Lobes are seen to thin and fine from lobe axis to lobe fringe becoming more structured with the occurrence of debrites in the lower part.

- Facies transitions in lobes generally show an increase in bed stratification and tractional structures from axial to fringe settings. However, this is not a linear transition because multiple zones of increased bed amalgamation are identified along strike. In general, net:gross decreases from axis to fringe as the lobe thins. However, not all lobes pass from axis to fringe in the same manner. No clear pattern in the style of thinning has been documented, although we speculate that lobes that thin and fine are less confined by underlying topography than those that maintain a structureless sandstone facies.

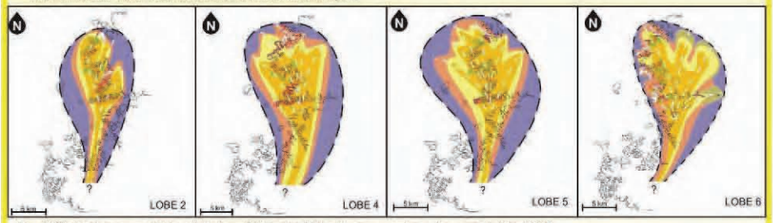

Fig. B2.2: Facies maps of lobes 2, 4, 5 and 6. Facies follow the same colour scheme as in Fig. B.2.2

Four broad environments of deposition in distributive systems have been identified for each element in the hierarchy: axis, off-axis, fringe, and distal fringe. Margin is avoided as this term has connotations with a confining surface.

- ***Axis settings*** are represented by >80% net: gross successions comprising amalgamated sandstone with local dewatering features, but no erosional confinement
- ***Off-axis settings*** are represented by 60-80% net: gross succession comprising stratified medium-bedded facies with Ta, Tab, and local Tc intervals, and some amalgamation. Some lenticular bedforms are identified here.
- ***Fringe settings*** are represented by 40-60% net: gross with medium- to thin-bedded successions of current ripple-laminated and/or bipartite and tripartite hybrid beds (linked debrites)
- ***Distal fringe settings*** are represented by <40% net: gross successions with thin-bedded very fine-grained sandstone and siltstone intervals that are commonly graded and ripple laminated.

B3. Shape

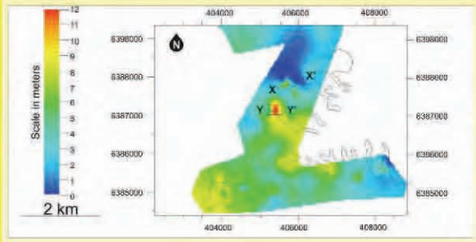

Fig. B3.1: ***Isopach maps*** were created from logged sections collected throughout the study area. Compilation of isopachs maps for each lobe and interlobe allow analysis of thickness variation, and construction of isopach maps.

Lobes are not simple radial bodies thinning evenly from the ceontroid (volumetric centre) as in an ellipsoid. Lobe 2, for example, in distal reaches is characterised by abrupt changes in thickness across strike.

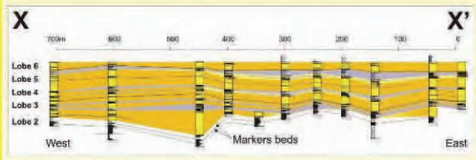

Fig. B3.2: **XX'** Lobe 2 thins from 3 m in the west to 0,1 m and then thickens back to 3 m moving east along strike. The cross-sectional geometry of this feature at outcrop is channel-form (base concave-up). Underlying marker beds are not truncated and follow the concave-up base of the lobe.

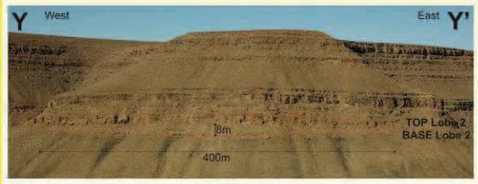

Fig. B3.3: **YY'** Up dip (500 m to the SW) along the same finger, Lobe 2 thickens to 14 m with a concave-up basal surface. Changes in thickness are abrupt and perpendicular to flow direction. Lobes that overlie the fingered basal lobe display minimal thickness variations.

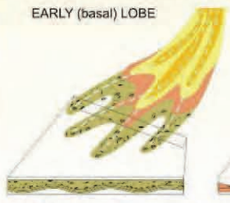

Fig. B3.4:Cartoon of early and late lobe and cross section through distal positions.

The pinchout pattern of Lobe 2 described above has a multiple finger-like expression. A similar pattern has been identified in basal lobes in Fan 3 in the Klipfontein area (lobe 4, this study), Fan 2 (Rozman 2000) and Fan 4 (Bouma and Rozman 2000). ***This finger-like pinchout pattern is particularly evident in basal lobes***, and indicates that the map view shape of lobes is not as smooth and radial as previously envisaged but can be much more irregular across strike. In contrast, the lateral fringe of lobe 6 is smooth and is parallel to the direction of thinning of the lobe, oriented N165. Away from its western fringe, lobe 6 thickens consistently at 2m/km.

B4. Stacking patterns

Local compensational stacking patterns

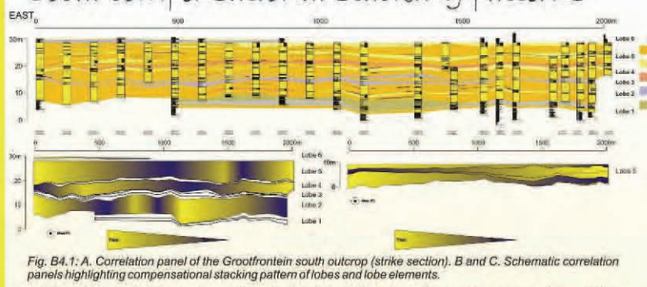

Fig. B4.1: A. Correlation panel of the Grootfontein south outcrop (strike section). B and C. Schematic correlation panels highlighting compensational stacking pattern of lobes and lobe elements.

- At outcrop, the compensational stacking of lobes is most apparent in strike orientated sections and can be demonstrated along a 2 km strike section in the Grootfontein area by the thickening and thinning patterns of lobes (2, 4 and 5).
- The maximum depositional relief is calculated by assuming that thickness change is due to seabed topography, and these estimates are presented as angles.
- From east to west, lobe 2 thins from 7.8 m to 4.2 m over 700 m (angle of 0.29°), thickens back to 10 m in 500 m (angle of 0.66°) and, at the western end, thins to 6.7m in 600m (angle of 0.32°). Locally, lobe 4 is thickest overlying the thinner parts of lobe 2, and thins from 5.4 m to 3.2 m over 1000 m to the east (angle of 0.13°). Finally, lobe 5 has two loci of thickening situated at either end of the panel and thickens from 6 m to 9 m in 1000 m towards the east and the west (angle of 0.17°).

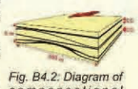

Fig. B4.2: Diagram of compensational cycles after Mutti and Sonnino, 1981. Scale is indicative.

Planform stacking patterns

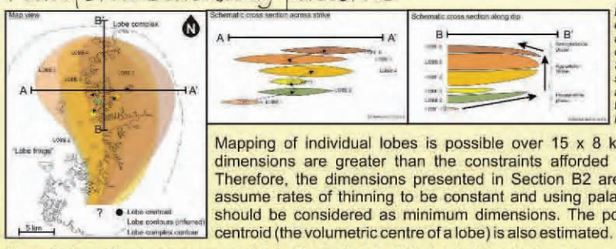

Fig. B4.3: Geometry of lobes within Fan 3 and stacking patterns of Lobes 2 to 6. Schematic cross section across strike and and along dip through the 6 lobes of Fan 3

Mapping of individual lobes is possible over 15 x 8 km, but a lobe's dimensions are greater than the constraints afforded by the outcrop. Therefore, the dimensions presented in Section B2 are estimates that assume rates of thinning to be constant and using palaeocurrents, and should be considered as minimum dimensions. The position of a lobe centroid (the volumetric centre of a lobe) is also estimated.

Nevertheless, the outcrop constraints indicate that the lobes are elongate in a down-dip direction with dimensions of several kilometres in length and width. Isopach maps, generated from logged thicknesses of lobes show a specific volume, position, and shape for each lobe within the field area.

B5. Dimensions

Methodology:

2D data, such as the lengths of surfaces, beds, bedsets, or 'shales', can be extracted easily from outcrop panels, but need to be reoriented from their outcrop lengths to be tied to local palaeocurrent directions.

Key conclusions:

- Interlobe low permeability intervals (thin-bedded fine-grained facies) were deposited as a blanket over lobes to form significant barriers to vertical fluid flow that are cut out locally

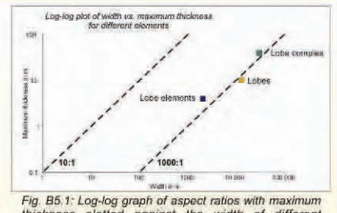

Fig. B5.1: Log-log graph of aspect ratios with maximum thickness plotted against the width of different architectural elements from Tanqua.

- Bed thickness distributions form segmented power laws, which is related to bed amalgamation and lobe element confinement
- Width to length ratios show a linear relationship across the hierarchy of lobe components (Fig. B2.2.)
- A non-linear relationship exists between lobe element thickness and lobe element area, which indicates the presence of a process that limits lobe element thickness to <3m (Fig. B2.3.)
- Aspect ratios (width to thickness) of lobe elements, lobes, and lobe complexes are comparable (1000:1)
- Estimates of typical turbidity current volumes and number of beds that comprise lobe elements have been calculated and used to help constrain process-based numerical models (Poster D)

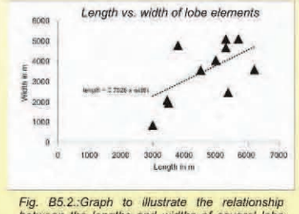

Fig. B5.2.:Graph to illustrate the relationship between the lengths and widths of several lobe elements identified in the Tanqua depocentre.

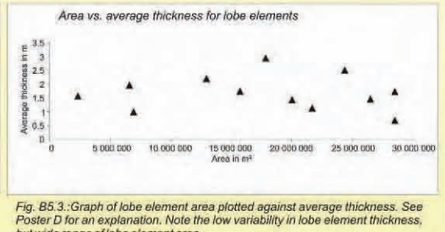

Fig. B5.3.:Graph of lobe element area plotted against average thickness. See Poster D for an explanation. Note the low variability in lobe element thickness, but wide range of lobe element area.

C. RESERVOIR MODELLING AND SUBSURFACE APPLICATION

Why geological reservoir modelling?
Modelling allows the visualisation of subsurface data in 3D that would not normally be visible in seismic data. Lateral facies variations is highlighted by the process, making the simulation of fluid flow possible. Digital outcrop models (DOM) provide a means to capture quantitative 1D, 2D ,and rarely 3D, data collected at outcrop.

1. Input data: vertical profiles measured in the study area includes information on sedimentary structures, architectural elements, bed thickness, facies, etc. This data can be visually represented as sedimentary logs and correlation panels in CorelDraw to highlight variation in stratigraphy, architecture and facies distribution.

2. Output data: input data is imported and manipulated in Petrel to build a 3D representation of the 2D outcrop data. The accuracy of the representation is dependant on the efficacy of the outcrop data for use in modelling software.

The work presented below forms part of theses by Jaco Neethling (C1) and Rochelle Steyn (C2), University of Stellenbosch.

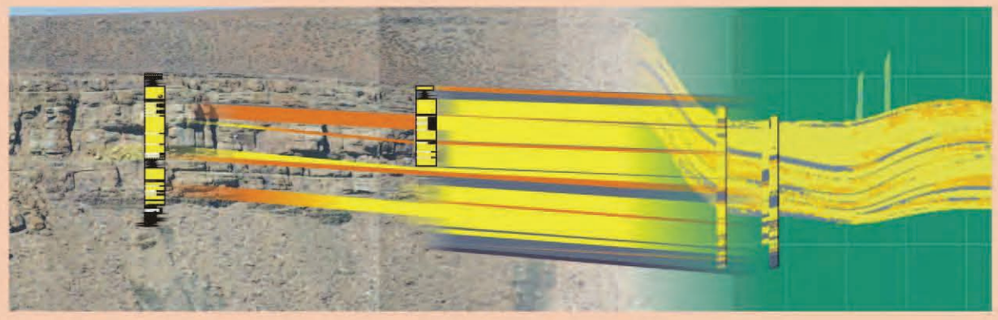

C1. lobe complex axis (Fan 3)

Outcrop observation

Outcrops of the **Fan 3 lobe complex** in medial axial position show a slightly different pattern to the outcrops studies to the north (Poster B). Lobe 3 is not present, and two additional lobes are present beneath Lobe 1. Lobes 2, 4 and 5 can be divided into **Upper** and **Lower lobe elements**, each exhibiting significantly different behaviour. For instance, Upper Lobe 5 pinches out 4 kilometres before Lower Lobe 5, and has a different palaeoflow direction. The outcrop below (Fig C1.1) represents the **southern Gemsbok valley**. Beneath are two correlation panels, one created in **CorelDraw** and the other a **Petrel** generated panel, both indicating facies variation across the 3800km long outcrop.

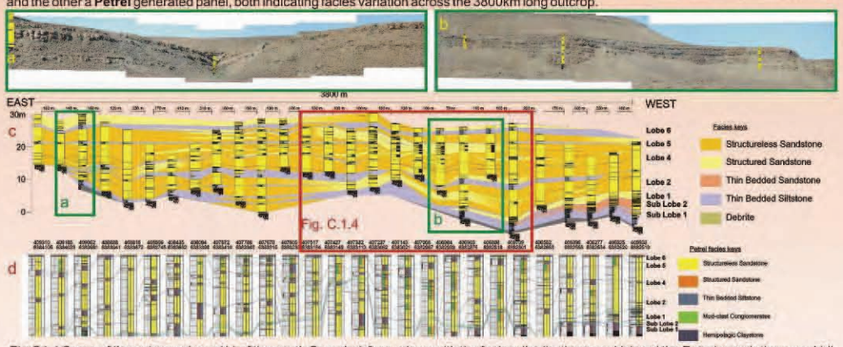

Fig.C1.1 Some of the outcrops (a and b) of the south Gemsbok face, along with the facies distribution panel (c) and the Petrel correlation panel (d).

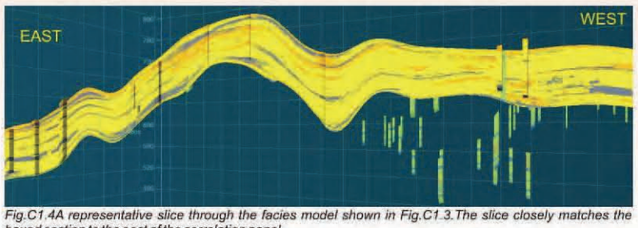

Fig.C1.4A representative slice through the facies model shown in Fig.C1.3.The slice closely matches the boxed section to the east of the correlation panel.

3D Geological model

A **conceptual depositional model** was constructed using outcrop data and **isopachs** created in Petrel. The conceptual model was converted into a **grid** in Petrel and divided into 19 **zones** based on the **top and base surfaces** of lobes and lobe elements. The internal variation was simulated using **proportional layering**. Surface **topography** was left unchanged.

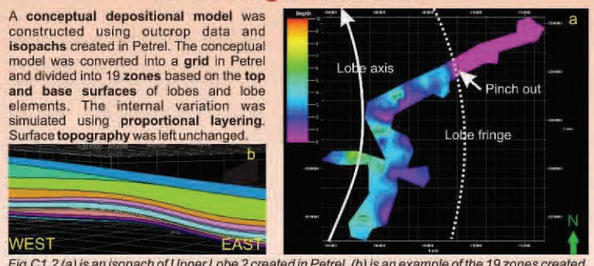

Fig.C1.2 (a) is an isopach of Upper Lobe 2 created in Petrel. (b) is an example of the 19 zones created. The zones represent 4 lobes, with 6 lobe elements (upper and lower lobes) and 9 interlobe units).

Reservoir model

The wells were upscaled into the 20mx20m **cells** of the grid, and the 3D distribution was simulated in 3D by using the **sequential Gaussian algorithm**.
The model is shown in Fig C1.3

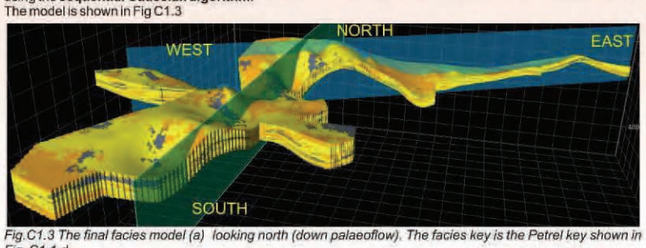

Fig.C1.3 The final facies model (a) looking north (down palaeoflow). The facies key is the Petrel key shown in Fig. C1.1.d.

C2. Lobe axis to fringe (Middle Fan 2)

Outcrop observation

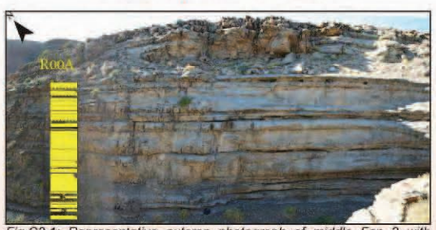

*Fig.C2.1: Representative outcrop photograph of middle Fan 2 with **vertical profile R00A** on the farm Kleine Gemsbok Fontein. Ninety-one vertical profiles were measured, representing Middle Fan 2 outcrop across the study area. Each profile depicts observations on sedimentary structures, facies and architectural elements.*

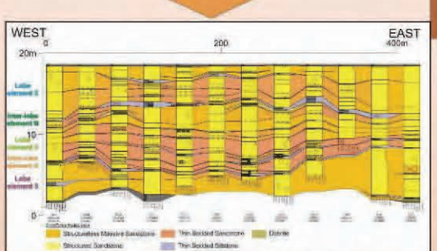

*Fig.C2.2: Correlation panel created using **CorelDraw,** illustrating the internal variation between 12 vertical profiles measured adjacent to each other on the farm Kleine Gemsbok Fontein. Middle Fan 2 is subdivided into three sandstone lobe elements separated by siltstone inter-lobe elements.*

3D geological model

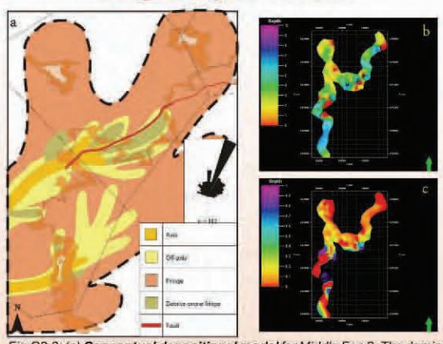

*Fig.C2.3: (a) **Conceptual depositional model** for Middle Fan 2. The dominant palaeocurrent indicates flow to the north-east. Isopach thickness maps were created for lobe element 1 (b) and inter-lobe element B (c), with hot colours indicating **thinner** elements .*

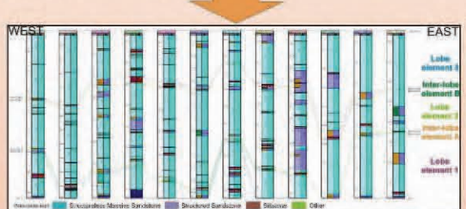

*Fig.C2.4: Correlation panel created using **Petrel,** illustrating the difference between input outcrop data (left) and output upscaled data (right). Input data represents 17 original facies, output data represents facies reduced to 5.*

Reservoir model

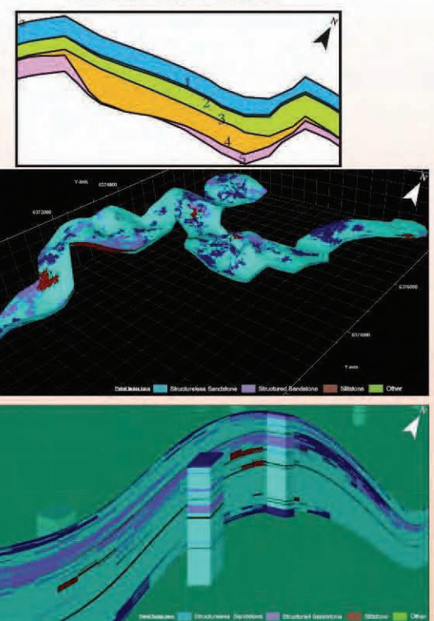

*Fig.C2.5: **Reservoir model** for Middle Fan 2 indicating the lobe elements and inter-lobe elements represented by 5 zones, each subdivided into layers (a), (b and c) the facies model for Middle Fan 2 and detail of the upscaled facies in the facies model.*

D. AUTOGENIC CONTROLS ON THE GEOMETRY AND STACKING PATTERN OF TERMINAL LOBE DEPOSITS

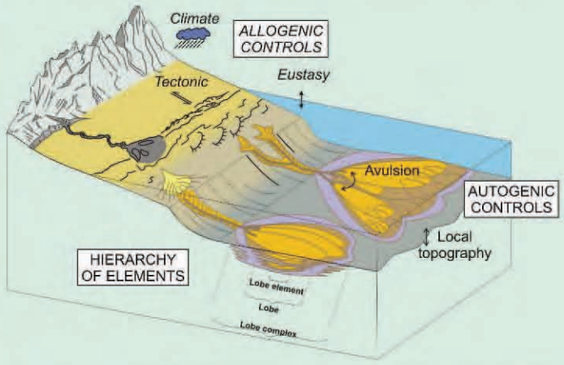

The architecture of submarine fans is governed by a multitude of processes, some of which may be classified as allogenic to a fan system, whereas others are considered autogenic.

Allogenic, or extrinsic, controls are those that force change in the architecture of the fan system *from the outside*. Examples of allogenic controls are mostly related to changes in the sediment supply signal (volume and frequency of flows, grain size of the source sediment), e.g., due to changes in relative sea level and climate, and changes in seafloor shelf-slope morphology due to tectonic activity.

Autogenic, or intrinsic, controls are those that cause changes in architecture due to processes occurring *in the fan system itself*. Autogenic behaviour in submarine fans is intimately related to the interplay between turbidity-current flow and sedimentation, which causes a subtle but complicated and dynamic depositional topography that strongly impacts the loci of erosion and deposition of subsequent flows and, therefore, the facies and thickness distributions of architectural elements.

D1. Finger like lobe geometry

Outcrop observation

Outcrops of Fan 3 demonstrate that planform geometries of lobes are not simple radial fan shapes. Commonly, lobes have finger-like projections near their termination, particularly basal lobes on a muddy substrate (see Section B3).

Interpretation

This cartoon map represents facies and thickness distributions within a typical Tanqua lobe. It attempts to **synthesise outcrop observations, isopach maps, and correlation panels.** There are no 'hard' lines between facies as these are transitional, and dotted lines represent axial pathways and indicate that there is not a single axis to a lobe. Smooth radial isopach contour lines are sketched here although in reality they are more complicated, particularly in areas close to pinchout.

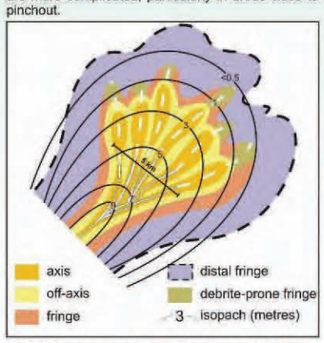

Fig D.1.1.:Cartoon map to represent facies and thickness distributions within a typical Tanqua lobe.

Process-based realisation

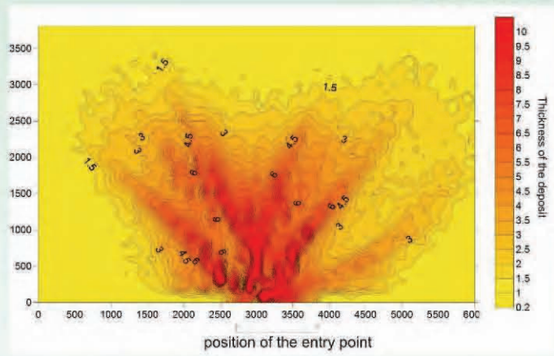

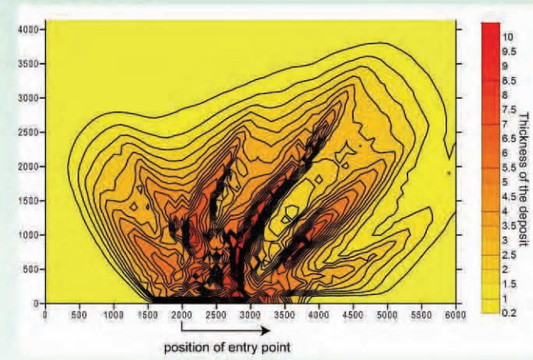

Aim:
To mimic the lateral shifts in the position of the mouth of a distributary channel due to avulsion, or a change in the axis of flow through a (depositional) shallow conduit. The position of the entry point of the flows into the model domain was varied on a flow-by-flow basis and in a disorganized manner.

Inflow position:
Inflow positions were randomly assigned from a distribution with a mean of 3000m and a standard deviation of 200 m. As such, all flows entered the domain of interest roughly between 2400 and 3600m.

Result:
Clearly, the disorganized shift in entry point results in an asymmetric stacking of beds which causes the depositional relief to be undulating, with elongated highs and lows in-between that widen downstream. Properties of this simulated lobe, such as the number of beds, overall thickness, volume and geometry, are in agreement with those observed at lobe scale in outcrop.

Aim:
To assess the influence of a more organized way of entry point switching, both in time and in space.

Inflow position:
The input parameters values are the same than in the previous example, but with flow entry points shifting from 2000 m to 3400 m and with steps of 100 m. Timing of the shifts was defined such that a shift occurred every three to four flows, depending on size and recurrence interval, which are randomly drawn from user-defined log normal distributions.

Result:
Elongate ridges now vary in length, and curve towards the right, i.e., in the direction of lateral shift of the entry point. Furthermore, flows seem to have preferentially followed one particular conduit, which therefore has resulted in bounding highs left and right that are more pronounced than the other highs, and also in transport of sediment further downstream. Evidently, the more organized shift of entry point, both in time and space, has resulted in a depositional relief with more pronounced highs with lows in-between that serve as pathways for several consecutive flows, which increases the distance over which sediment is transported.

D2. Compensational stacking patterns

Outcrop observation

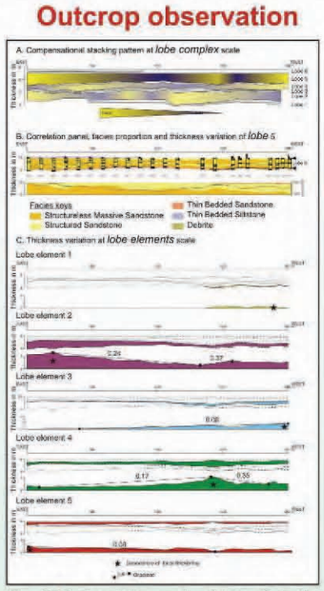

Fig. D2.1: Correlation panel of Lobe 5 in the Grootfontein area (strike section) and schematic correlation panels of individual lobe elements, highlighting distinct local thickening and thinning at lobe element scale, which is interpreted to result from the interaction of flows with depositional relief (compensational stacking).

Interpretation

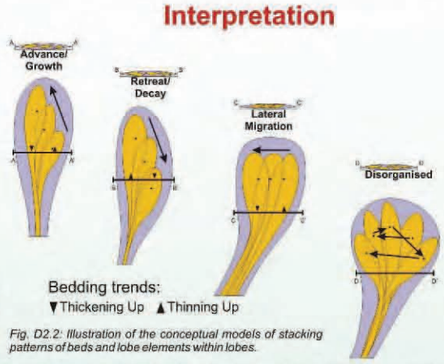

Fig. D2.2: Illustration of the conceptual models of stacking patterns of beds and lobe elements within lobes.

Four simple conceptual models of different lobe element stacking styles that can occur during the formation of a lobe, advance, retreat, lateral, disorganised.

Stacking Style 1: Advancement or Growth
This style could develop where the up-dip distributary channel is increasing in efficiency (channel lengthening) and/or sediment supply rate increases, although it could develop as an autogenic response to dynamic underlying topography.

Stacking Style 2: Retreat or Decay
This style could develop where the up-dip distributary channel is decreasing in efficiency (channel shortening) and/or sediment supply rate decreases, although it could develop as an autogenic response to dynamic underlying topography.

Stacking Style 3: Lateral Migration
This style could develop where sediment supply is quasi-stable, but the position of the distributary channel moves laterally (avulsion or open channel migration).

Stacking Style 4: Disorganised
This style could develop where the position of the up-dip distributary channel and/or the rate of sediment supply are unstable, although it could develop as an autogenic response to the developing underlying topography.

Process-based realisation

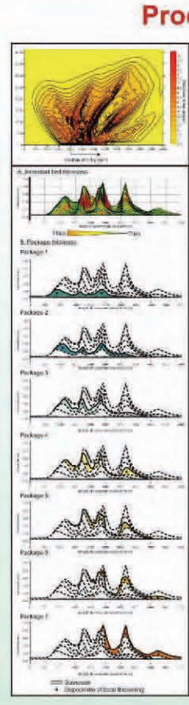

← *Fig. D2.3:* The cross-section is located at 900 m downstream of the entry point of the flows. The cross-section at the top displays the stratigraphy, with colour coding representing individual bed thickness. In the other cross-sections, individual beds have been grouped into 7 packages, based this time on the position of the entry point of the flows that deposited them, to highlight the effect of a systematic change in the position of a distributary channel-mouth or depositional conduit on the distribution of sediment and, consequently, organised stacking pattern at the scale of packages of beds. Each package is roughly equivalent in number of beds and volume to two lobe elements.

Fig. D2.4: →
The cross-section is located at 2200 m downstream of the entry point of the flows. The cross-section A displays the stratigraphy, with colour coding representing individual bed thickness. In the other cross-sections (B), individual beds have been grouped into four packages, based on spatial trends in bed thickness and grain size to illustrate lateral shifts in the locus of deposition due to the disorganized shift in entry points and the interaction of flows with depositional relief. Packages are equivalent in volume and number of beds to two to three outcrop-defined lobe elements. After Package 1, at any given time, deposition never occurs in a single area, i.e., it occurs simultaneously both to the left and right of Package 1, although at different rates.

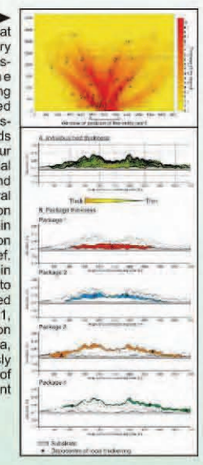

E. DISCUSSIONS AND CONLUSIONS

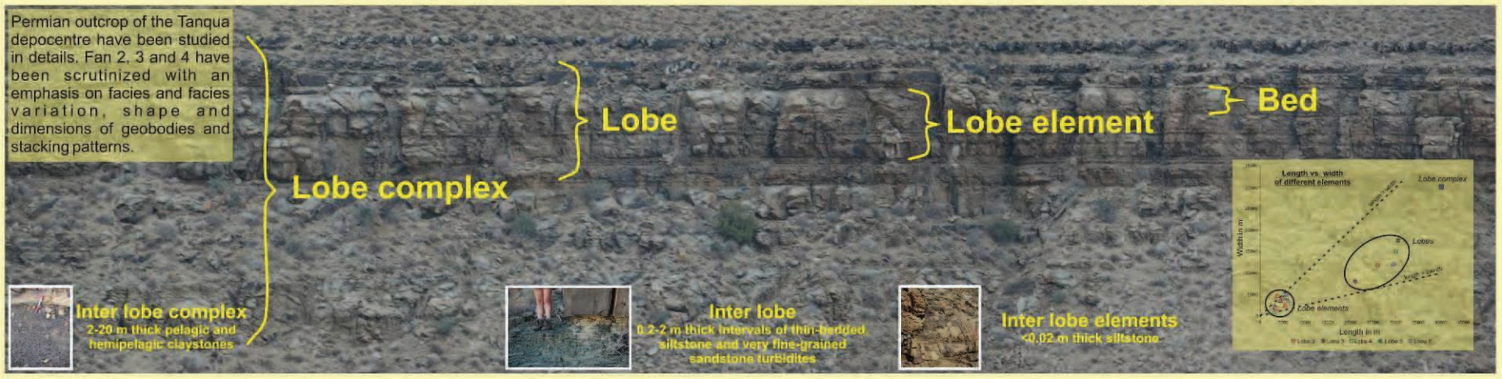

B. OUTCROP DATASET

Here, Digital Outcrop Models was built only after conceptual depositional models of the distributive systems had been developed (B). Outcrop data was used to narrow input parameters for a processed-based numerical model that was validated with the outcrop observations. The numerical model was used iteratively to test hypotheses and to refine the conceptual model (D). The refined conceptual depositional model and the quantitative data collected from the outcrops were used to construct 3D geological (reservoir) models, which can be used as a check on the conceptual model. Seismic data and physical model was not incorporated to refine the depositional model further.

Narrow input parameters

Model validation

iteration

Refine conceptual models

Hypothesis testing

Quantitative data: 1D, 2D, and 3D

Test field obs

Conceptual depositional model

D. NUMERICAL MODEL

Constrain o/c uncertainties

Hypothesis testing

C. RESERVOIR MODEL

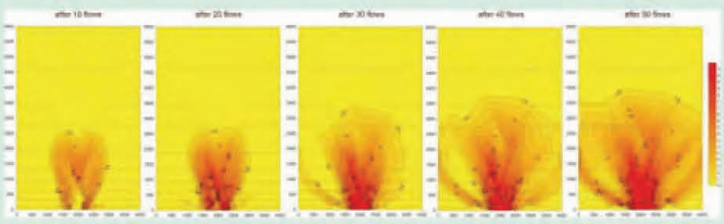

Outcrop studies give a good insight on turbidite reservoirs at interwells scale. However, the results obtained are mostly specific to the fan system under investigation, and extrapolation of findings to other fan systems often proves challenging. The 'process-based' approach focuses on the turbidity currents themselves. In addition, process-based numerical models provide a means to test and develop hypotheses developed from outcrop

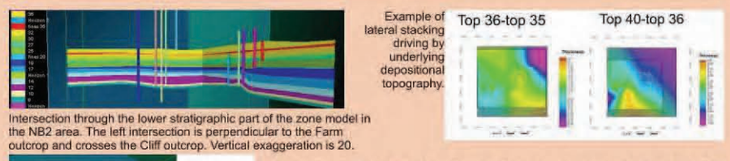

Intersection through the lower stratigraphic part of the zone model in the NB2 area. The left intersection is perpendicular to the Farm outcrop and crosses the Cliff outcrop. Vertical exaggeration is 20.

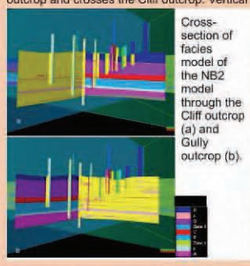

Cross-section of facies model of the NB2 model through the Cliff outcrop (a) and Gully outcrop (b).

The zone model for the NB2 area (built by Wieske Paulissen, TU Delft) represents several levels in the hierarchy of the lobe complex, and may provide insights into the trends of the zones and their stacking patterns. Since the NB2 model is based on a high-resolution field dataset it was possible to model a lobe element in one zone in the lower part of the stratigraphy and in one case even an individual bed (unit 36). Up stratigraphy, thicker packages were modelled in one zone which are lobes embedded in continuous siltstone- and mudstone-prone intervals.

E4. References

Fildani, A., Drinkwater, N.J., Weislogel, A., McHargue, T., Hodgson, D.M, Flint S.S. (2007) Age controls on the Tanqua and Laingsburg deep-water systems: New insights on the evolution and sedimentary fill of the Karoo basin, South Africa Source: Journal of sedimentary research, 77, 901 -908

Twichell DC, Schwab WC, Kenyon NH (1995) Geometry of sandy deposits at the distal edge of the Mississippi fan, Gulf of Mexico. In: Pickering KT, Hiscott RN, Kenyon NH, Ricci Lucchi F, Smith RDA (eds) Atlas of deep water environments: architectural style in turbidite systems. Chapman and Hall, London, pp 282–286

Wickens H de V (1994) Basin floor fan building turbidites of the southwestern Karoo Basin, Permian Ecca Group, South Africa. PhD Thesis, Univ Port Elisabeth, 233 pp

E5. Acknowledgments

The authors wish to thanks the LOBE consortium: Chevron, Maersk Oil, Petrobras, Petro SA, Shell, StatoilHydro and Total for sponsorising several studenships. Most of the reservoir modelling with Petrel® licences provided by Schlumberger, and the work was completed at PetroSA Cape Town and we are especially grateful for the help we received from Jody Frewin. Laura McAllister, Emily Parrott and John Kavanagh are thanks for field assistance.